

Accepted Manuscript

Evaluation of bbb permeable nucleolipid ($n_{l_{dpu}}$): a di-c15-ketalised palmitone appended uridine as neuro-tracer for spect

Swastika, Shubhra Chaturvedi, Ankur Kaul, Puja Panwar Hazari, Preeti Jha, Sunil Pal, Sangeeta Lal, B Singh, Philippe Barthélémy, Anil K Mishra

PII: S0378-5173(19)30345-X
DOI: <https://doi.org/10.1016/j.ijpharm.2019.04.074>
Reference: IJP 18322

To appear in: *International Journal of Pharmaceutics*

Received Date: 6 December 2018
Revised Date: 16 April 2019
Accepted Date: 27 April 2019

Please cite this article as: Swastika, S. Chaturvedi, A. Kaul, P. Panwar Hazari, P. Jha, S. Pal, S. Lal, B. Singh, P. Barthélémy, A.K. Mishra, Evaluation of bbb permeable nucleolipid ($n_{l_{dpu}}$): a di-c15-ketalised palmitone appended uridine as neuro-tracer for spect, *International Journal of Pharmaceutics* (2019), doi: <https://doi.org/10.1016/j.ijpharm.2019.04.074>

This is a PDF file of an unedited manuscript that has been accepted for publication. As a service to our customers we are providing this early version of the manuscript. The manuscript will undergo copyediting, typesetting, and review of the resulting proof before it is published in its final form. Please note that during the production process errors may be discovered which could affect the content, and all legal disclaimers that apply to the journal pertain.



EVALUATION OF BBB PERMEABLE NUCLEOLIPID (NL_{DPU}): A DI-C15-KETALISED PALMITONE APPENDED URIDINE AS NEURO-TRACER FOR SPECT

Swastika,^{a,b} Shubhra Chaturvedi,^a Ankur Kaul,^a Puja Panwar Hazari,^a Preeti Jha,^a Sunil Pal,^a Sangeeta Lal,^c B Singh,^b Philippe Barthélémy,^{d,*} and Anil K Mishra ^{a,*}

^a*Division of Cyclotron and Radiopharmaceutical Sciences, Institute of Nuclear Medicine and Allied Sciences, Brig. S. K. Mazumdar Road, Delhi-110054, India*

^b*Department of Chemistry, Banaras Hindu University, Varanasi, Uttar Pradesh, India*

^c*School of Physical Sciences, Jawaharlal Nehru University, Delhi-110067*

^d*INSERM U1212 and Université de Bordeaux, Bordeaux, F-33076, France*

*Email: philippe.barthelemy@inserm.fr Phone No; 33 557 574 853

*Email: akmishra63@gmail.com Phone No: +011-23905117

ABSTRACT: Despite being in routine for onco-diagnostics for years, the applicability of nucleosidic molecular imaging probes is severely restricted in neurological applications due to their low permeability across blood-brain-barrier (BBB). For extending nucleoside tracers utility for neuro-onco early diagnostics, suitable modification which enhances their BBB permeation needs investigation. Among various modifications, lipidization of nucleosides has been reported to enhance cellular permeability. Extending the concept, the aim was to exemplify the possibility of lipidized nucleosides as potential brain tracer with capability to cross intact BBB and evaluate as metal based neuro-imaging SPECT agent. Uridine based non-lipidic (NS_{DAU}) and di-C15-ketal appended lipidic (NL_{DPU}) ligands were conjugated to chelator, DTPA (DTPA-NS_{DAU} and DTPA-NL_{DPU}) using multi-step chemistry. The ligands were evaluated in parallel for comparative physical and biological parameters. Additionally, effects of enhanced lipophilicity on UV-absorption, acid strength, fluorescence and non-specific protein binding were evaluated. Fluorescence quenching of BSA indicated appreciable interaction of DTPA-NL_{DPU} with protein only above 10 mM without inducing conformational changes. In addition, DTPA-NL_{DPU} was found to be haemato-compatible and cyto-compatible with low dose-dependent toxicity in HEK-cells. The chelator DTPA was used for ^{99m}Tc-complexation for SPECT imaging. Optimized ^{99m}Tc-radiolabeling parameters resulted in quantitative ($\geq 97\%$) labeling with good stability parameters in in-vitro serum and cysteine challenge studies. We demonstrate that the nucleolipid radiotracer (^{99m}Tc-DTPA-NL_{DPU}) was successfully able to permeate the BBB with brain uptake of 0.2% ID/g in normal mice as compared to 0.06% ID/g uptake of ^{99m}Tc-DTPA-NS_{DAU} at 5 min. Blood kinetics indicate biphasic profile and $t_{1/2}(\text{distribution})$ 46 min for ^{99m}Tc-DTPA-NL_{DPU}. The preferential accumulation of ^{99m}Tc-DTPA-NL_{DPU} in brain tumor intracranial xenograft indicate the targeting capability of the nucleoside. We conclude that as first-of-its-kind, this work presents the potential of the biocompatible nucleolipidic system for brain targeting and early diagnostics.

KEYWORDS: nucleolipid, radiotracer, brain-imaging, BBB permeable, SPECT imaging, nucleoside tracer.

1. INTRODUCTION

Imaging of metabolic alterations has been exploited extensively for the detection and assessment of therapeutic intervention in diseases particularly, cancer (Di Gialleonardo et al, 2016). The basis of metabolic molecular imaging is the metabolic reprogramming in tumors, inflammation-infection and neurodegenerative diseases (Demetrius et al., 2014; Levy and Bartosch , 2016; Gleeson and Sheedy, 2016). Enhanced uptake of metabolites in uncontrolled proliferating cells, like tumors, leads to a differential concentration in comparison to normal-cells which results in the required contrast for imaging. Among the metabolic tracers, the glucose analogue, fluorine labelled deoxy glucose (FDG), has been the major radiotracer for molecular imaging using positron emission tomography (PET) with applications in oncology, inflammation, and infections. FDG is preferentially retained at the diseased site due to enhanced glucose requirement and intracellular entrapment, resulting in required contrast for imaging (Alauddin, 2013). However, (1) the non-specific uptake in non-tumor sites particularly at inflammation and infection sites, (2) uncorrelated uptake with respect to cellular proliferation and (3) high background in certain tissues associated with high glucose metabolism like the brain, limits FDG application in oncological and neuro-oncology imaging, (Chen et al., 2005; Basu et al., 2009), in spite of FDG being permeable to intact blood-brain barrier (BBB) (Saha, 2004). Alternately, metabolic tracers based on nucleosides offered specificity and quantitative correlation of the tracer uptake with the growth rate of tumor. Nucleosides being the structural unit of nucleic acids have a high turnover in rapidly

proliferating cells viz., tumorigenic cells, proportional to the DNA synthesis (Alauddin, 2013).

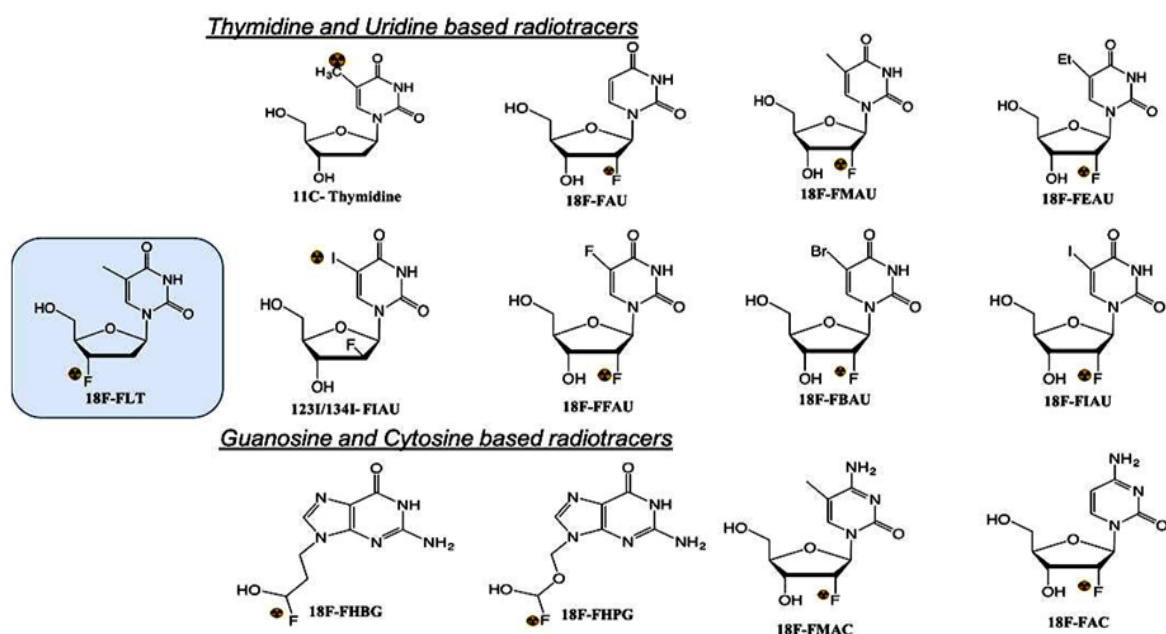


Figure 1: Well-known nucleoside-based probes for imaging with ^{18}F -FLT dominating the clinical application in onco-diagnostics: FLT: fluoro-labelled thymidine, FIAU or Fialuridine: 2'-fluoro-2'-deoxy-1-beta-D-arabinofuranosyl-5-iodouracil, FMAU: 1-(2'-Deoxy-2'-fluoro-beta-D-arabinofuranosyl)thymine, FFEAU: (1-(2'-deoxy-2'-fluoro-beta-D-arabinofuranosyl)-5-(2-fluoroethyl)uridine), FEAU: 2'-fluoro-5-ethyl-1-beta-D-arabinofuranosyluracil, FBAU: (2-deoxy-2-fluoro-beta-D-arabinofuranosyl)-5-bromouracil, FAC: 1-(2'-deoxy-2'-fluoro-beta-D-arabinofuranosyl)cytosine, FMAC: 1-(2'-deoxy-2'-fluoro-beta-D-arabinofuranosyl)-5-methylcytosine, FHBG: 9-(4-fluoro-3-hydroxymethylbutyl)guanine, FHPG: 9-((3-fluoro-1-hydroxy-2-propoxy)-methyl)guanine, FHOMP: 6-((1-fluoro-3-hydroxypropan-2-yloxy) methyl)-5-methylpyrimidine-2,4(1H,3H)-dione)

A gamut of nucleoside based radiotracers namely, derivatives of thymidine [^{18}F -FLT], uridine [$^{124}\text{I}/^{131}\text{I}$ -FIAU, $^{11}\text{C}/^{18}\text{F}$ -FMAU, ^{18}F -FFEAU, ^{18}F -FEAU, ^{18}F -FBAU], cytosine [^{18}F -FAC, ^{18}F -FMAC], guanosine [^{18}F -FHBG, ^{18}F -FHPG] and modified pyrimidines [FHOMP] have been developed for imaging of cancer (Figure 1, see caption for abbreviations; Alauddin, 2013; Meyer et al., 2014; Pysz and Willmann, 2014) The tracers varied in their ability to produce signals (tumor: background sensitivity), metabolic degradation and bio-distribution. Despite being studied and used routinely in clinics for oncologic diagnostics for past three-four decades, the utility of the

nucleosides probes (e.g. FLT) for delineation of low grade tumors having uncompromised BBB is severely restricted due to low permeability across the intact BBB (Chen et al., 2005). FLT (Chen et al., 2005; Alauddin, 2013; Meyer et al., 2014; Pysz and Willmann, 2014), FIAU, (Pysz and Willmann, 2014; Langen and Galldiks, 2016; Tehrani and Shields et al., 2013), FHBG (Langen and Galldiks, 2016), FHPG, (Langen and Galldiks, 2016) FEAU, FFEAU, (Miyagawa et al., 2008) FAC, FMAC, (Schwarzenberg et al., 2011) and FBAU (Kao et al., 2002) are known not to cross the BBB. In order to make the nucleosides radiotracers permeate through the intact BBB, lipophilic modifications of nucleosides were reported (Chaturvedi and Mishra, 2016). These lipophilic modifications included the introduction of di-benzoylation at 3' and 5' of FBAU (Kao et al., 2002) and vinylic substitution at 5' position of uridine in FIAU (Li et al., 2008). The results were promising with [76Br]-FBAU-3', 5'-dibenzoate having a brain uptake of 0.23%ID/g as opposed to brain uptake of only 0.08 %ID/g for [76Br]-FBAU. However, in case of the vinylic substitution in spite of enhanced lipophilicity, the brain accumulation of FIAU and vinylic-FIAU were similar. Lipidization of drugs has also been one of the approaches, to improve the cellular internalization and brain delivery (Zaro, 2015). Among promising lipid-drug conjugates are palmitoyl conjugated oxytocin derivative (LOT-1) (Mizuno et al., 2015) designed for enhance brain delivery, and docosahexanoic acid (DHA)-conjugated paclitaxel (Bedikian et al., 2010) having enhanced tumor uptake and improved pharmacokinetics. As an attempt to enhance cellular internalization, nucleosides have also been appended with long alkyl chains, resulting in nucleolipids (Rosemeyer, 2005; Gissot et al., 2008; Baillet et al., 2018). Initial leads in the structural design of nucleolipids came from the existence of naturally occurring conjugates like cytidine diphosphate diacylglycerol (CDP-diacylglycerol) in

biological systems. The early reports on the biomedical application of nucleolipids include modification of 1-(beta)-D-arabinofuranosylcytosine, an anticancer drug, as adamantane or palmitate derivatives to enhance cellular penetration and improve efficacy ((Rosemeyer et al., 2005). The N4-acyl derivatives of Arabinosylcytosine AraC, appended with C₁₅-C₂₂ saturated fatty acids, were shown to have better antitumor activity attributed to the enhanced cellular internalization and stability towards deaminases (Lansakara et al., 2012).

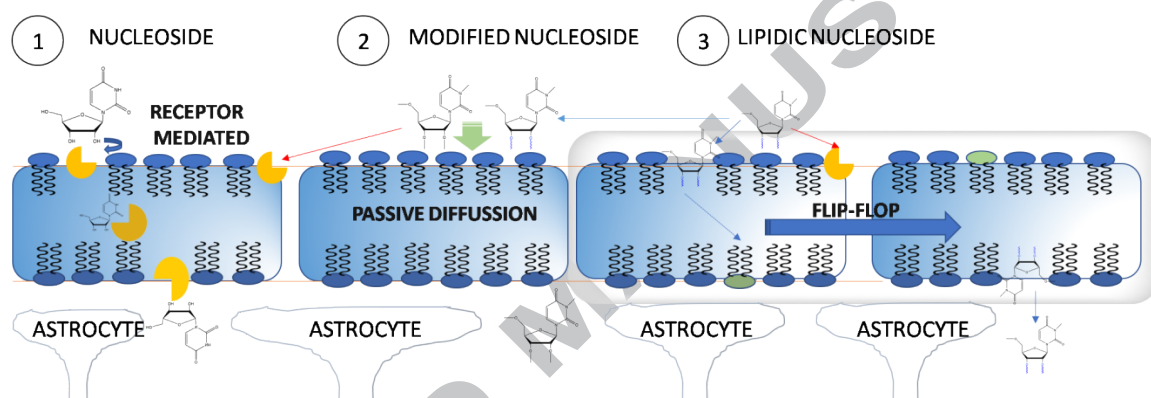


Figure 2 : Schematic representation of nucleoside internalizing through the blood-brain barrier (BBB) 1. Natural nucleoside primarily is transported across the BBB through receptor- mediated internalization 2. Modified nucleosides unrecognized by receptors rely on passive diffusion across the BBB 3. Lipidic nucleosides similar to modified nucleosides rely on mechanisms of passive diffusion, e.g. flip-flop across BBB.

Nucleosides permeate across cellular membrane through nucleoside transporters, whereas the enhanced cellular internalization of nucleolipids is due to the lipid moiety which mediates diffusion and flip-flop mechanism thereby accelerating the absorption of nucleolipids across cellular membranes (Scheidt et al., 2004; Allain et al., 2012; Zhu et al., 2013; Figure 2) Experimental evidence includes diffusion mediated cellular internalization of lipophilized gemcitabine derivatives in nucleoside transporter-hENT1 deficient cell line ((Lansakara et al., 2012; Baillet et al., 2018). Since lipidization is a well-established strategy for developing BBB permeating drugs, we hypothesize that the nucleolipid may prove to be effective in

delivering nucleoside-based radiotracer across BBB wherein nucleolipids act as (a) carrier molecule across BBB and also as (b) selective metabolite tracer due to the presence of nucleoside. In addition to being brain impermeable, majority of nucleoside-based tracers are halogen labelled [^{18}F for PET imaging and $^{76}\text{Br}/^{123}\text{I}$ for single photon emission computed tomography (SPECT) imaging]. ^{76}Br or ^{123}I labelled tracers are liable to undergo dehalogenation as primary degradation mode thereby limiting biological use. ^{18}F labelled tracers have limited dehalogenation but the short half-life of 109.7 min and high operational cost associated with ^{18}F production using on-site cyclotron limit its applicability, especially in remote areas. Metal-based tracers are attractive alternatives as the radionuclides for imaging viz., ^{68}Ga and $^{99\text{m}}\text{Tc}$ are generator based thereby having a lower economic burden which can have higher societal implications. (Chaturvedi et al., 2017)

For biological application, the metal-based tracers require a strong chelator to be appended with the ligand which results in stable metal complexes with low probability of transchelation reaction with the biological molecules. The polyaminocarboxylic acid derived chelators like diethylenetriaminepentaacetic acid (DTPA), undergo fast and high yielding metal complexation. DTPA is a known chelator for ^{68}Ga (PET), $^{99\text{m}}\text{Tc}$ (SPECT), ^{111}In (SPECT) and also Gd^{+3} (Magnetic Resonance Imaging (MRI)), Tb^{+3} and Eu^{+3} (Optical imaging) thereby allowing operational versatility to the radiotracer by changing the metal ion. (Li et al., 1995; Saha, 2004; Liu et al., 2008).

As an attempt to enhance the brain-penetrating ability of the nucleosides, we have evaluated the potential of the uridine based nucleolipid (NL_{DPU}) having two C_{15} chains for brain penetration. NL_{DPU} has been conjugated with DTPA which serves as the chelator for the radionuclide $^{99\text{m}}\text{Tc}$, thereby resulting in $^{99\text{m}}\text{Tc}$ -DTPA- NL_{DPU} . For comparison, non-lipidic uridine (NS_{DAU}) derivative ($^{99\text{m}}\text{Tc}$ -DTPA- NS_{DAU}) has also been evaluated. The results indicate enhanced brain penetrating properties of $^{99\text{m}}\text{Tc}$ -DTPA- NL_{DPU} and its possible

application for brain imaging. Though we have evaluated the proposed system as SPECT tracer, the ligand can find application as tracer for any of the molecular imaging modality- PET/SPECT/MRI or optical imaging by virtue of the versatile nature of the chelator.

2. MATERIALS AND METHODS

2.1 Synthesis and characterization

Chemicals:

Uridine, tosylic acid, tosyl anhydride, triethyl orthoformate, sodium bicarbonate, triethyl amine, chloroform, sodium azide, pyridine, dimethyl formamide, palladium on activated charcoal 10%, dry methanol and DTPA bis anhydride were purchased from Sigma-Aldrich Co., USA. Palmitone (16-hentriacontanone) was purchased from TCI Chemicals, India. Silica gel mesh size 80-120 for column chromatography was procured from Merck, Germany. Concentrated sulphuric acid, diethylenetriaminopentaacetic acid, stannous chloride, stannous tartrate, sodium bicarbonate, 3-(4, 5- dimethylthiazol-2-yl)2, 5-diphenyltetrazolium bromide (MTT), sulfo-rhodamine B (SRB) dye, glacial acetic acid, Trichloroacetic acid (TCA), pyridine, Bovine serum albumin (BSA) were purchased from Sigma Aldrich, St Louis, MO, USA. All other chemicals used were of the standard analytical grade. Glass wares used were oven-dried.

Characterization:

^1H and ^{13}C - NMR spectra were recorded on Bruker Avance II 400 MHz and Bruker Avance 600 MHz using deuterated solvents procured from Merck, Germany at 298 K using 10-15 mg compound. Chemical shifts are reported in ppm and referenced to the solvent residual peak. Mass Spectroscopy data was acquired using electrospray ionization-mass spectrometry (ESI-MS) on Agilent 6310 ion trap fitted with Agilent 1200 LC (M/S Agilent Germany). Lyophilization was performed on M/S Labconco system.

2.1.1. Synthesis of DTPA-NS_{DAU}**2', 3'-O-Isopropylidene Uridine (1a)**

The synthesis was carried as already reported with minor modifications (Levene and Tipson, 1934). In brief, uridine (2.042 mol, 500 mg) was dissolved in 20 mL of acetone containing 4 Å molecular sieves. Sequential addition of anhydrous copper sulphate (5.10 mmol, 814.99 mg) and 0.025 mL of conc. sulphuric acid (diluted in 5 mL acetone) was carried. The solution was stirred at room temperature for 48 h. The reaction solution was filtered to remove copper sulphate, and the filtrate was evaporated under vacuum. The compound was obtained as white foam. Percent yield 73.14% (TLC: R_f 0.5 in ethyl acetate)

¹H-NMR (400 MHz; (CD₃)₂-SO) δH: 11.37 (1 H, brs, -NH), 7.78 (1 H, d, J ≈ 8 Hz : H-6), 5.81 (1 H, d, J ≈ 2 Hz : H-1'), 5.62 (1 H, dd, J ≈ 8 Hz : H-5), 4.87 (1 H, d: -CH_{uridine}), 4.72 (1 H, d: -CH_{uridine}), 4.05 (1 H m: -CH_{uridine}), 3.58 (2H, m : H-5'), 3.32 (1 H, br : -OH), 1.46-1.26 (6 H; 2×-CH₃)

¹³C-NMR (100 MHz; (CD₃)₂-SO) δc: 163.29, 150.40, 142.01, 113.02, 101.78, 91.20, 86.58, 83.76, 80.53, 61.32, 27.00, 25.20

MS (ESI-): m/z calcd for C₁₂H₁₆N₂O₆ [M]: 284.27: found 283 [M-H]-

5'-Azido-5'-Deoxy-2', 3'-O-Isopropylidene Uridine (2a)

2',3'-O-Isopropylidene Uridine (1a) (1.76 mmol, 500 mg) was suspended in dichloromethane (10 mL). Addition of pyridine (5 mL) dissolved the compound completely. The solution was cooled in an ice-bath. Tosyl chloride (2.28 mmol, 435.36 mg) was added in small batches. The reaction was left overnight on stirring. The solution was concentrated in vacuum and the crude mixture obtained was used as such. The mixture was then reacted with sodium azide (5.13 mmol, 334 mg) in 15 mL dimethylformamide (DMF) and refluxed for 8 h. After evaporation under vacuum, yellow-colored oil was obtained. Purification on silica gel column

chromatography using hexane/ EtOAc lead to the desired compound as white solid (TLC: Rf 0.2 in hexane/ EtOAc 1:1).

$^1\text{H-NMR}$ (400 MHz; CDCl_3 (0.3% TMS)) δH : 10.03 (1 H, brs, -NH), 7.241 (1 H, d, H-6), 5.71 (1 H, t, H-1'), 5.62 (1 H, J=2.4 Hz: H-5), 4.95 (1 H, m: -CHuridine), 4.74 (m, 1H: -CHuridine), 4.17 (1 H, m: -CHuridine), 3.56 (2 H, m, 5'-CH₂), 1.51-1.09 (6 H, 2 \times CH₃).

$^{13}\text{C-NMR}$ (100 MHz; CDCl_3 (0.3% TMS)) δc : 162.98, 149.50, 142.24, 114.84, 102.86, 94.62, 85.66, 84.28, 81.42, 52.32, 27.09, 25.23

MS (ESI-): m/z calcd for $\text{C}_{12}\text{H}_{16}\text{N}_2\text{O}_6$ [M]: 309.28: found 309.54

5'-Amino-5'-Deoxy-2', 3'-O-Isopropylidene Uridine (3a)

5'-Azido-5'-Deoxy-2',3'-O-Isopropylidene Uridine (2a) (1.61 mmol, 500 mg) was dissolved in dry methanol (20 mL) under an inert atmosphere (nitrogen) in ice-bath. After brief stirring, hydrogen gas was bubbled into it using long needle syringe. Palladium (10% activated on charcoal) was added in a catalytic amount (137 mg, 1.29 mmol). Adequate precautions were exercised to avoid contact of the catalyst with air. The reaction was stirred for 6 h and allowed to attain room temperature. For separating palladium, the reaction mixture was poured over celite bed and washed thrice with methanol. On drying the filtrate, light yellow powder with a yield of 80% was obtained (TLC: Rf 0.3 in hexane/EtOAc 1:1).

$^1\text{H NMR}$ (400 MHz; CDCl_3 (0.3% TMS)) δH : 9.7 (1 H, brs, -NH), 7.23 (1 H, d: H-6), 5.75 (1 H, d, J=8.4Hz: H-5), 5.59 (1 H, J=2Hz: H-1'), 4.93 (1 H, m: -CHuridine), 4.75(1 H, m: -CHuridine), 4.18 (1 H, m: -CHuridine), 3.56 (2 H, m, 5'), 3.05(2 H, brs, -NH₂), 1.5-1.18 (6 H, 2 \times CH₃)

$^{13}\text{C-NMR}$ (100 MHz; CDCl_3 (0.3% TMS)) δc :163.79, 150.12, 142.58, 114.68, 102.73, 84.30, 84.23, 82.07, 81.43, 44.14, 25.13, 24.59

MS (ESI-): m/z calcd for $\text{C}_{12}\text{H}_{16}\text{N}_2\text{O}_6$ [M]-: 283.28: found 282.9[M-H]-

5'-DTPA-5'Deoxy-2', 3'-O-Isopropylidene Uridine (4a)

5'-Amino-5'Deoxy-2', 3'-O-Isopropylidene Uridine (3a) (500 mg, 1.766 mmol) was dissolved in 5 ml anhyd DMF and stirred. To this, solution of DTPA bis anhydride (630 mg, 1.766 mmol) in anhyd DMF (10 mL) was added drop-wise. The pH of the reaction mixture was adjusted to 8 using triethylamine and the contents were refluxed at 80° C for 48 h. The progress of the reaction was monitored by TLC in ethyl acetate and 0.2% methanol. The compound with a yield 54 % was obtained as white solid after precipitating in acetone and diethyl ether (TLC: Rf 0.43 in ethyl acetate and 0.2% methanol)

¹H-NMR (400 MHz; (CD₃)₂-SO) δH: 10.54 (brs : 4x-COOH DTPA), 7.94 (brs: -NH_{DAU}), 7.66 (1H, brs, -NHamide), 7.30 (1H, s: H-6), 5.73-5.62 (2H : H-1', H-5), 4.82-3.73 (4H: -CHuridine), 3.19 (4H, br, 5'-H, 1X-CH₂,DTPA), 2.89-2.79(m, 8H, 4X-CH₂,DTPA), 1.89 (8H, s, 4X-CH₂,DTPA), 1.06 (6H, 2X-CH₃)

¹³C-NMR (100 MHz; (CD₃)₂-SO) δc: 174.46, 168.63, 163.47, 163.36, 158.64, 154.13, 151.51, 144.16, 140.41, 135.33, 130.14, 113.31, 103.01, 87.04, 86.12, 85.56, 71.75, 56.16, 55.26, 36.35, 25.54.

MS (ESI-): m/z calcd for C₂₆H₃₈N₆O₁₄ [M]-: 658.24: found 656.1 [M-2H]-

2.1.2 Synthesis of DTPA-NL_{DPU}

2', 3'-O-16-hentriacontanyliden-uridine (1b)

The compound was synthesized as per the already mentioned protocol (Gissot et al., 2008). Uridine (5.54 mmol, 1.35 g) was dissolved in 20 ml of tetrahydrofuran. Sequential addition of 16-hentriacontanone (1.11 mmol, 500mg), triethylorthoformate (0.933 ml, 5.54 mmol, 822.51 mg) and tosylic acid monohydrate (TsOH.H₂O: 1.11 mmol, 211.1 mg) was carried, and the

solution was refluxed for 24 h. After 24 h, the reaction was quenched by addition of 2 ml of triethylamine. The reaction solution was then poured over ice and sodium bicarbonate (4 g) and stirred briefly. The compound was extracted in dichloromethane. The yellow colored organic layer was collected and dried over sodium sulfate. After evaporation under reduced pressure, crude solid (yield 62%) was obtained. Further, purification on silica column with hexane/ EtOAc gave the desired product as white solid. (TLC: Rf 0.4 in hexane/ EtOAc 1:1).

$^1\text{H-NMR}$ (400 MHz; CDCl_3 (0.3% TMS)) δH 9.13 (1 H, brs, -NH), 7.33 (1 H, d, J 8 Hz: H-6), 5.76 (1 H, d, J 8Hz: H-5), 5.54 (1 H, dd, J 2 Hz: H-1'), 5.02 (1 H, d: -CHuridine), 4.95 (1 H, d: -CHuridine), 4.27 (1 H, m: -CHuridine), 3.91 (2H, dd : H-5'), 2.90 (1 H, br : -OH), 1.74-1.26 (56 H; Lipidic chain)

$^{13}\text{C-NMR}$ (100 MHz; CDCl_3 (0.3% TMS)) δc : 163.07, 150.26, 143.08, 118.45, 102.60, 96.35, 87.22, 83.83, 80.29, 62.70, 31.90, 29.82, 29.68, 29.64, 29.56, 29.34, 24.16, 23.56, 22.662, 14.091

5'-Azido-5'-Deoxy-2', 3'-O-16-hentriacontanyliden-uridine (2b)

Compound 1(b) (1, 1.18 mmol, 800 mg) was tosylated using tosyl chloride (1.77 mmol, 354 mg) in pyridine (5 mL) and dichloromethane (10 mL) overnight at ice-cold conditions. After evaporation under reduced pressure, the crude compound was obtained which was taken further without purification. The tosylated compound was then reacted with sodium azide (2.406 mmol, 156 mg) in 15 mL dimethylformamide (DMF) and refluxed for 8 h. The reaction mixture was evaporated, and the yellow-colored compound was obtained. Further purification on silica gel column chromatography using hexane-EtOAc leads to the desired compound as white solid (yield 86%, Rf 0.6 in hexane: EtOAc 2:1).

$^1\text{H-NMR}$ (400 MHz; CDCl_3 (0.3% TMS)) δH : 9.32 (br, 1H, -NH), 7.20 (1H, d, H-6), 5.68 (1H, d, 1'), 5.56 (1H, d, H-5, $J=6\text{Hz}$), 4.942 (1 H, d: -CHuridine), 4.72(1 H, d: -CHuridine), 4.155 (1 H, d: -CHuridine), 3.535 (2H, m, 5'), 1.71-0.88 (56 H)

$^{13}\text{C-NMR}$ (100 MHz; CDCl_3 (0.3% TMS)) δc : 163.00, 149.85, 142.66, 118.73, 102.79, 95.28, 86.096, 84.48, 52.41, 36.90, 31.90, 29.79, 29.337, 24.11, 22.67, 13.76

MS (ESI-): m/z calcd for $\text{C}_{40}\text{H}_{71}\text{N}_5\text{O}_5$ [M-]: 701.5: found 701.2

5'-Amino-5'Deoxy-2', 3'-O-16-hentriacontanyliden-uridine (3b)

Compound 2(b) (0.541 mmol, 380mg) was dissolved in dry methanol under an inert atmosphere (Nitrogen) in ice- bath. After brief stirring, hydrogen gas was bubbled into it. Palladium (10% activated on charcoal) was added in a catalytic amount (34 mg, 0.324 mmol). Adequate precautions were exercised to avoid contact of the catalyst with air. The reaction was stirred for 6 h and allowed to attain room temperature. The reaction mixture was poured over celite bed and washed with methanol. On drying the filtrate, the white powdery product was obtained. Further purification by column chromatography on silica gel using hexane: EtOAc as eluent, gave the desired product as white solid (R_f 0.43 in hexane: EtOAc 1:1).

$^1\text{H-NMR}$ (400 MHz; CDCl_3 (0.3% TMS)) δH :9.30 (1H, brs, -NH), 7.17 (1H, s, H-6), 5.75 (1H, H-1'), 5.54 (1H, d, H-5), 4.93 (1H, m: -CHuridine), 4.74 (m, 1H: -CHuridine), 4.20 (1 H, m: -CHuridine), 3.51(2H, m, 5'), 1.65 (2H, brs, -NH₂),1.34-0.83 (56 H, Lipidic chain)

$^{13}\text{C-NMR}$ (100 MHz; CDCl_3 (0.3% TMS)) δc : 141.33, 139.27, 117.96, 114.07, 102.30, 94.01, 85.89, 85.27, 81.21, 78.87, 69.96, 58.59, 50.57, 37.02, 36.96, 33.83, 32.11, 31.94, 29.17, 14.13

MS (ESI+): m/z calcd for $\text{C}_{40}\text{H}_{73}\text{N}_3\text{O}_5$ [M] +: 676.02: found 676.8[M] +, 690.8 [M+Na] +

5'-DTPA-5'Deoxy-2', 3'- O-16-hentriacontanyliden-uridine (4b)

Compound 4 (0.512 mmol, 350 mg) was dissolved in 5 ml anhyd DMF and stirred. To this, a solution of DTPA bis-anhydride (218.9 mg, 0.612 mmol) in anhyd.DMF (10 mL) was added drop wise. The pH of the reaction mixture was adjusted to 8 using triethylamine and refluxed at 80° C for 48 h. The progress of the reaction was monitored by TLC in ethyl acetate and 0.2% methanol. The compound was obtained as white solid after precipitating in acetone and characterised.

¹H-NMR (400 MHz; (CD₃)₂-SO) δH :11.40-10.30 (brs : 4x-COOHDTPA), 7.73 (2H, m: H-6, -CONH), 6.045 (1H, d: H-1') 5.71 (1H, brs, -NHamide), 5.59 (2H: H-5), 4.96 (m, 1H: -CHuridine), 4.68 (1 H: -CHuridine), 4.57 (1H: -CHuridine), 4.28 (1H: -CHuridine), 3.90 (2H, br, 5'-H), 3.45 (10H, 5-CH₂,DTPA), 2.89-2.99 (m, 8H, 4X-CH₂,DTPA), 1.21 (48 H, 2X-CH₂, 24 CH₂ -Lipidic Chain), 0.82-0.81 (6H, 2X-CH₃)

¹³C-NMR (100 MHz; (CD₃)₂-SO) δc :178.70, 176.30, 174.70, 172.64, 160.28, 154.80, 149.81, 143.63, 142.46, 139.42, 115.79, 79.23, 60.04, 45.77, 39.99, 31.40, 30.81, 29.53, 29.11, 28.90, 28.81, 22.21, 17.70, 14.06

MS (ESI-): m/z calcd for C₅₄H₉₄N₆O₁₄ [M]: 1050.3: found 1050.8

2.2 Physicochemical characterization

UV Spectroscopy:

Varying concentrations of ligands (DTPA-NS_{DAU} and DTPA-NL_{DPU}) were prepared in Millipore water, and the UV spectra (180-700 nm) were recorded on Synergy 2 Multi-mode reader (M/S BioTek Instruments, USA). For comparison, compounds DTPA-NS_{DAU} and DTPA-NL_{DPU} were analyzed under similar conditions. In all calculations, the water background was subtracted from the sample.

Potentiometric titrations:

Direct potentiometric titrations were performed for 0.1 M ligands (DTPA-NS_{DAU} and DTPA-NL_{DPU}) against 0.01 M Tetrabutylammonium hydroxide (TBAOH) using a Metrohm ion

analysis potentiometer fitted with a pH meter-electrode system, calibrated for pH 4, 7 and 9 before performing the experiment.

2.3 Protein binding assessment by Fluorescence quenching:

Fluorescence studies:

In order to study the protein binding by fluorescence quenching, fluorescence characteristics of the ligands (DTPA-NS_{DAU} and DTPA-NL_{DPU}) were established. Fluorescence emission spectrum of varying concentrations (0.5 mM- 12.5 mM) of the ligands was recorded from 300-700 nm on Synergy 2 Multi-mode reader (M/S BioTek Instruments, USA) with excitation at 280 nm.

Fluorescence Quenching:

The experiment was conducted as reported previously with minor modifications (Mingxiong et al., 2013). 0.1 mM Bovine Serum Albumin (BSA) stock solution, solutions and dilutions of ligands (DTPA-NS_{DAU} and DTPA-NL_{DPU}) were prepared in 1X Tris buffer solution. In a 96 well black opaque plate, 100 μ L of BSA was incubated with different concentrations of the ligands. The final volume in each well was 200 μ L. The solutions were mixed thoroughly by gentle pipetting. The mixture was allowed to stand for 5 min. The fluorescence spectrum from 300-700 nm was recorded using Synergy 2 Multi-mode reader (M/S BioTek Instruments, USA) with excitation at 280 nm. 100 μ L BSA with 100 μ L buffer served as negative control which gave the maximum fluorescence intensity. The experiments were conducted at room temperature, and Tris buffer background was subtracted.

Each measurement was carried in triplicates. The data obtained was fitted in the following graphs for the evaluation of parameters. In order to establish the quenching mechanism of the ligands on BSA, Stern-Volmer equation was used for analysis.

$$\frac{F_0}{F} = 1 + K_{sv}[Q]$$

where: F_0 = Fluorescence intensity of pure BSA (negative control) : F = Fluorescence intensity of BSA + analog: K_{sv} = biomolecular quenching constant: $[Q]$ =molar concentration of quencher (ligand)

Binding constant and number of binding site

The binding constant and the number of binding sites were evaluated using the equation:

$$\text{Log} \frac{F_0 - F}{F} = n \text{Log}[Q] + \text{Log}K$$

where: F_0 = Fluorescence intensity of pure BSA (negative control): F = Fluorescence intensity of BSA+ analog: K =binding constant: $[Q]$ =molar concentration of quencher (analog): n = number of binding sites

For the calculation of parameters, the data was plotted as $\text{Log} ((F_0-F)/F)$ against concentration of quencher $\text{Log} [Q]$. K and n were calculated from the intercept and the slope respectively.

2.4 Toxicity Assessment:

2.4.1 Haemo-compatibility using haemolysis activity:

Haemolytic assessment of the ligands (DTPA-NS_{DAU} and DTPA-NL_{DPU}) was done using red blood cells (RBC) from a heparinized human blood samples following previously reported protocols with minor modifications (Dumoga et al., 2017). In order to separate the RBCs from the plasma, the samples were centrifuged at 3000 rpm for 10 min at 4°C. The RBC pellet was washed thrice with saline (pH 7.4) to decolorize and suspended in 50 mL of phosphate buffered saline (pH 7.4) to form an RBC suspension. Aliquots of RBCs (1.8 mL) were added with 0.2 mL of the 2.5 mM ligands to have a final concentration of 0.25 mM. After thorough, gentle mixing, the samples were incubated for required time at 37°C. For

evaluation of time-dependent haemolytic action of the compound, the samples were evaluated at different time points (1 h, 2 h, 3 h and 4 h) wherein after the required time interval, the samples were centrifuged at 3000 rpm at 4°C for 10 min. The end point was the destruction of the RBSs, qualitatively evident from the extent of red coloration and quantitatively measurable by measuring the optical density of the supernatant at 540 nm using Synergy 2 Multi-mode reader (M/S BioTek Instruments, USA). Positive and negative control samples contained Triton X-100 (2% v/v) and saline respectively. In Triton X-100 treated RBCs, intense red coloration due to free haemoglobin was observed which indicated maximum haemolysis, also evident by the maximum absorbance at 540 nm. Percent haemolysis was calculated by the following equation:

$$\%Haemolysis = \frac{Abs\ sample, \lambda 540nm}{Abs(triton\chi - 100, \lambda 540nm)} = 100$$

2.4.2 Cyto-toxicity using cell line:

Cell Culture: Human embryonic kidney (HEK) cell lines were procured from National Centre for Cell Science (NCCS) Pune, India. The cell line was cultured in high glucose DMEM supplemented with 10% fetal bovine serum (FBS) and antibiotics: 1% (v/v) penicillin-streptomycin. The cell line was maintained in humidified 5% CO₂ incubator at 37° C. Cells were routinely sub-cultured twice a week using 0.05% trypsin in 0.02% EDTA.

SRB assay was performed to find the cytotoxicity of the compound DTPA-NL_{DPU} using HEK cell lines. The procedure was adopted as reported previously with minor modifications (Khurana et al., 2015). Cells were seeded at the density of 5000 cells per well in 96 well microtiter plate. Cells were treated with 0.02 mL of varying concentration (0.0001 μM-1000 μM) of DTPA-NL_{DPU} for different time intervals (24, 48 and 72 h). After the incubation for intended time, the wells were emptied, and the cells were fixed with 100 μL of ice cold 10% (w/v) trichloroacetic acid (TCA) for 1 h at 4°C. This was followed by four washings of the

well with water. Plates were then air dried and 100 μL of 0.05 % SRB solution was added in the well for 30 min for staining. Plates were quickly rinsed four times with 1% (v/v) acetic acid to remove excess unbound dye and air dried. Bound protein stain was solubilised using 200 μL of 10 mM Tris base solution (pH 10.5), and the plate was shaken on the gyratory shaker for 5 to 10 min. In the positive control, the cells were treated with HBSS (Hank's Balanced Salt Solution) buffer instead of the compound and treated exactly similar as described above. The color intensity was measured fluorometrically at excitation 488 nm and emission at 585 nm on Biotek Synergy H4 hybrid multiplate reader. The surviving fraction was calculated and plotted against the concentration range (0.001 μM -1000 μM) as a function of time.

2.5 Radiolabelling and stability parameters:

$^{99\text{m}}\text{Tc}$ -pertechnetate was procured from Board of Radiation and Isotope Technology (BRIT), Delhi, India. Since $^{99\text{m}}\text{Tc}$ is a gamma emitting radionuclide ($E_{\gamma}=140.5$ keV), adequate precautions were taken while it's handling. Radioactive counts were recorded on the well counter (Caprac R Capintec, USA) calibrated for $^{99\text{m}}\text{Tc}$ energy.

2.5.1 Radiolabelling

The ligands (DTPA-NS_{DAU} and DTPA-NL_{DPU}) were radiolabelled with $^{99\text{m}}\text{Tc}$ using the standard procedure with slight alterations (Spies et al., 2007) and various radiolabeling parameters were optimized to attain high labelling efficiency and radiochemical purity. The parameters include stannous tartrate concentration and incubation time. In brief, following procedure was followed. Freshly prepared stannous tartrate (0.43 mg/mL in 10 % acetic acid) was added to 300 μl of (4a and 4b) (2.8 nmol). The pH was adjusted to 7.0 with 1 M Na₂CO₃. $^{99\text{m}}\text{Tc}$ -pertechnetate (380 \pm 10 MBq) was added and incubated for 1 h at room temperature. Ascending instant thin-layer chromatography using silica gel-coated fiber sheets

(ITLC-SG) (Gelman Science Inc., Ann Arbor, MI, USA) were used for evaluating labeling efficiency and radiochemical purity. Radiolabeling efficiency was confirmed by thin layer chromatography (TLC) wherein free pertechnetate with an R_f of 0.9–1.0, migrates to the top portion of the strip and the labelled complex ($^{99m}\text{Tc-DTPA-NS}_{\text{DAU}}$ or $^{99m}\text{Tc-DTPA-NL}_{\text{DPU}}$) and $^{99m}\text{Tc-colloids}$ if any remains at the bottom when the mobile phase is 100% acetone. $^{99m}\text{Tc-colloids}$ were estimated by running ITLC in pyridine: acetic acid: water combination (3:5:1.5) wherein the radiolabeled complex and free pertechnetate migrated at the top leaving colloids at the bottom. The radioactivity in different regions of the TLC strip was determined by the gamma counter.

2.5.2 Log P value determination:

The lipophilicity parameter (log P) value was determined as the ratio of the concentration of compound between n-octanol and water (pH 7.4). The logarithmic value of the partition coefficient is defined as Log P. Briefly the analog was dissolved in 1 mL water and solubilized. To this an equal volume of n-octanol was added and the mixture was shaken vigorously on the vortex shaker for 10 min. The mixture was laid aside so that the layers separate. After proper separation of the layers, the concentration of the compound was measured in 100 μL of the two layers. The experiments were performed in triplicates.

For unlabelled ligands, $\text{DTPA-NS}_{\text{DAU}}$ and $\text{DTPA-NL}_{\text{DPU}}$, the lipophilicity parameter was evaluated by measuring the absorbance at 260 nm for both layers.

$$\text{Lipophilicity parameter} = \text{Log}P = \text{Log}\left(\frac{\text{Abs}_{\lambda 260, \text{Octanol}}}{\text{Abs}_{\lambda 260, \text{Water}}}\right)$$

For the radiolabelled complex ($^{99m}\text{Tc-DTPA-NS}_{\text{DAU}}$ and $^{99m}\text{Tc-DTPA-NL}_{\text{DPU}}$), approximately 7.2 ± 1.3 MBq of the labelled compound was diluted in PBS, pH 7.4. To this, equal volume of 1-octanol was added. After vortexing and separation, as above, radioactive counts were measured in 100 μL of the two layers using a well-type gamma counter, and the following equation was used:

$$\text{Lipophilicity parameter} = \text{Log } P = \text{Log} \left[\frac{\text{Counts}(\text{Octanol})}{\text{Counts}(\text{Water})} \right]$$

In Vitro Serum Stability:

The radiolabelled compound was assessed for in-vitro stability through serum stability assay. Freshly collected human serum was incubated with 0.1 mL of radiolabelled compound (0.3 MBq) at 37 °C for varying time points. After desired incubation time (viz., 0.5-24 h), the samples were spotted on an ITLC-SG. ITLC-SG was analysed as described previously in the Radiolabelling section.

2.5.3 Cysteine challenge studies:

For challenge studies using cysteine, samples comprised of 0.5 mL of the radiolabelled complex (0.3 MBq, 0.5 mg) in PBS mixed with 1 mL of cysteine solution of varying concentration (25, 50, 100 mM in water). After incubation of 2 h at 37°C, aliquots from the samples were spotted on an ITLC-SG strip. The strip was developed in 0.1 M PBS wherein the complex was at the bottom whereas radiolabelled cysteine had an Rf of 0.73. The ITLC was analyzed as described previously in the radiolabeling section.

2.6 In Vivo Evaluation and Pharmacokinetics

Experimental Animals and Ethical statement:

The studies have been carried on female Balb/c mice (aged 2 months, weighing 25 ± 2 g) and New Zealand albino rabbits (weighing 2-3 kg). The animals were housed in the INMAS experimental animal house facility in sterile cages and pathogen-free conditions. They were fed ad libitum with standard food and water, maintained at 22-25°C with a 12 h day and night cycle. The experiments have been performed as per the guidelines of INMAS Institutional Animal ethics committee (Reg no.8/GO/a/99/CPCSEA). New Zealand rabbits were used for blood clearance studies. BALB/c mice were used for imaging and bio-distribution studies.

Intracranial brain mice U87-MG xenograft:

Human brain tumor xenografts were developed using human primary glioblastoma cell line (U87-MG) as reported. (Ozawa and James., 2010). A serum- free single U87-MG cell suspension (1×10^5 in 30 μL of saline) was used for intracranial cell implantation in ketamine-xylazine anaesthetized athymic mice using use a small animal stereotactic frame. The injection depth was controlled to have an injection at 3 mm from the underside of the skull. After injection using Hamilton syringe 27 gauge, the skull was cleaned and the scalp was sutured. Proper post-operative care including pain relief with diclofenac was carried. The mice were monitored to regain normal activity and growth for 1 week. Visual inspection of the intracranial xenograft in mice revealed no signs of inflammation, which indicated no leakage of the cell line in the cranium of the mice. Histopathological studies of formalin-fixed mice brain slices ascertained the tumor growth.

2.6.1 Blood kinetics studies:

Blood Kinetics studies are carried in normal New Zealand rabbits. The complexes ($^{99\text{m}}\text{Tc}$ -DTPA-NS_{DAU}: 6 MBq, 1.5 mg in 1 mL and $^{99\text{m}}\text{Tc}$ - DTPA-NL_{DPU}: 7.5 MBq, 1.5 mg in 1 mL) were administered intravenously through the dorsal ear vein of the animal. From the other ear's vein, blood samples were collected at different time intervals. Activity associated was counted using well shape gamma counter (Caprac R Capintec, USA). The radioactivity in blood circulation after decay correction was expressed as a percentage of the total activity in blood volume, taking 7.2% of the total body weight as the total weight of the blood. The logarithm of the percent radioactivity vs. the time post-injection was used to evaluate the distribution and elimination parameters. The rate constants for distribution and elimination (α and β respectively) were evaluated by the slope of the regression line. The intercepts were used to evaluate C_0 . The half-life corresponding to the distribution and elimination phases were calculated as per the following.

$$t_{1/2,distribution} = \frac{0.693}{\alpha}$$

$$t_{1/2,elimination} = \frac{0.693}{\beta}$$

2.6.2 Bio-evaluation

2.6.2.1 Bio-distribution in Normal Mice:

The biodistribution studies of ^{99m}Tc -DTPA-NS_{DAU} and ^{99m}Tc -DTPA-NL_{DPU} was performed in BALB/c mice under similar condition in order to have a comparative evaluation. In order to have a time-dependent profile, bio-distribution studies were carried at different time points. Mice were taken in triplicates in 4 different groups depending upon the different time points (viz., 5 min, 15 min, 60 min and 120 min). For each time point, 20 μL of the radiolabelled complexes: ^{99m}Tc -DTPA-NS_{DAU} (10.3 ± 3.7 MBq) and ^{99m}Tc -DTPA-NL_{DPU} (11.1 ± 2.7 MBq) was carefully injected into the tail vein of mice. At intended time post-injection, mice were sacrificed through the cardiac puncture, and different organs and tissues were dissected out using the dissection kit. The organs of interest were removed, made free from adhering tissues by rinsing in saline, collected in RIA vials and weighed. The radioactivity was calculated by measuring radioactive counts in the gamma well counter. Uptake of the radiotracer in each tissue was calculated and expressed as a percentage injected dose per gram of the tissue (% ID/g) and corrected for ^{99m}Tc decay.

2.6.2.2 SPECT Imaging in Xenograft

SPECT imaging of the xenograft was carried in dual head camera after injecting 100 μL of the radiolabelled complexes: ^{99m}Tc -DTPA-NS_{DAU} (35 ± 1.8 MBq) and ^{99m}Tc -DTPA-NL_{DPU} (34 ± 2.2 MBq) into the tail vein of athymic mice. Semiquantitative analyses were assessed using Amide 1.0.4.

3. RESULT AND DISCUSSION

Design of the Nucleolipid

The work aims to explore the potential of nucleolipid as imaging agent capable of penetrating BBB. Uridine was conjugated with two chains of C₁₅ saturated alkyl chain using 16-hentriacontanone or palmitone at the 2'-3' position of uridine using ketal linkage.

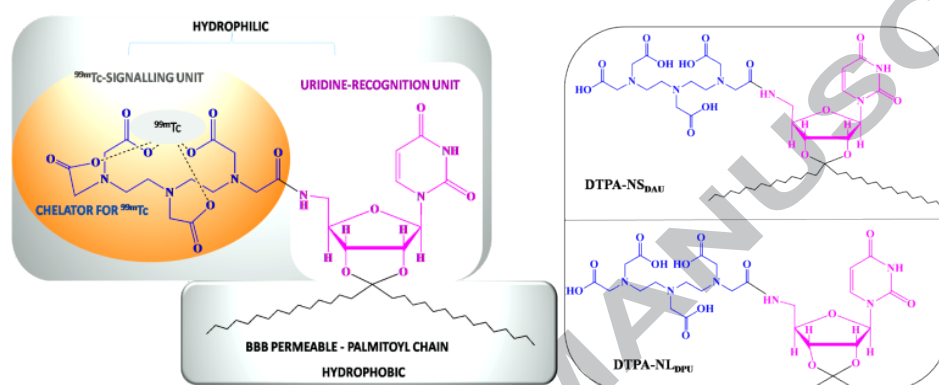


Figure 3: General design of ligands showing various units with their respective roles and general structure of ligands DTPA-NS_{DAU} and DTPA-NL_{DPU}

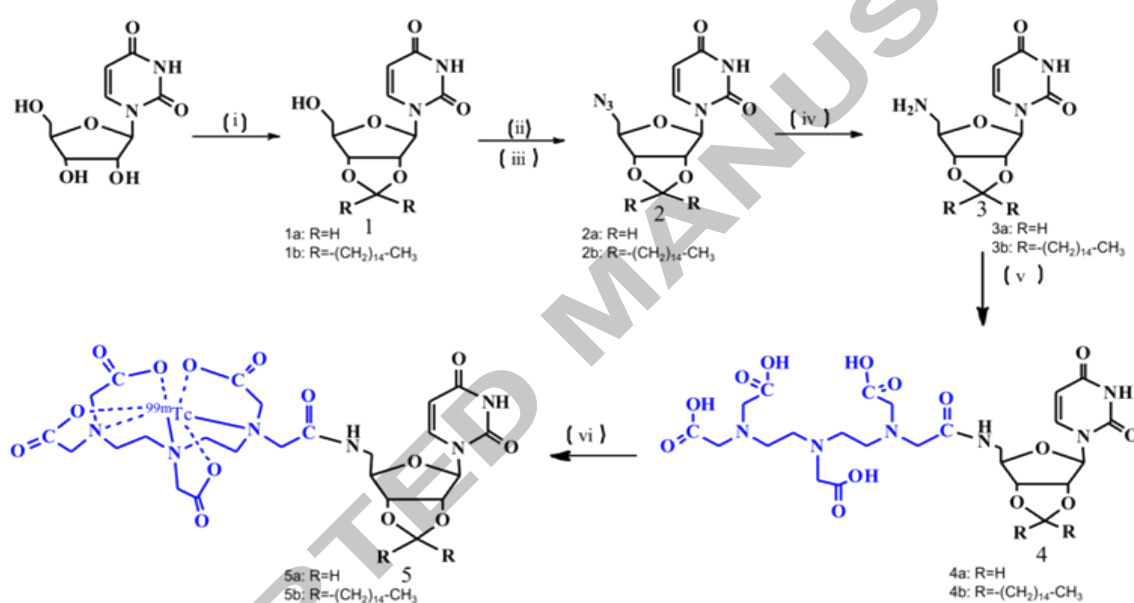
For an effective flip-flop to take place the alkyl chain should be comparable to the phospholipids forming unilamellar vesicles, and the membrane phospholipids are in the range C₁₄-C₂₂, (Spector, et al., 1985) C₁₅ alkyl chain was selected. In the past, palmitate (C₁₅) has been used to study fatty acid uptake and metabolism in the brain (Robinson et al., 1992), as well as conjugated with drugs to improve cellular internalization or brain delivery along with improved pharmacokinetics. Examples include palmitoyl conjugated oxytocin (LOT-1: Mizuno et al., 2015) with improved efficacy and oligonucleotide GRN 163 (GRN163L: Herbert et al., 2005) with the ability to internalize into cells without transfection facilitators. In order to modify the nucleolipid as a SPECT tracer, the nucleolipid had to be functionalized with chelator so that it can be loaded with ^{99m}Tc metal-radionuclide. The acyclic chelator, DTPA was preferred as it is an excellent chelator for ^{99m}Tc and reported extensively for the development of various ^{99m}Tc-based radiopharmaceuticals.⁸ ^{99m}Tc-DTPA, pertechnetate is

commonly used as a radiotracer for renal functioning, gastro-emptying, and imaging of the brain with the compromised BBB (Zolle, et al.,2007). Thus, an overall scheme (Scheme 1) was designed in which nucleoside conjugated with lipid was appended with DTPA to be later radiolabelled with ^{99m}Tc and evaluated as brain targeting tracer. In order to see the effect of the lipidic chain, the non-lipidic nucleoside was also appended to DTPA and evaluated similarly as lipidic-nucleoside-DTPA conjugate. The general design of ligands is shown in Figure 3.

3.1 Synthesis and Characterization:

The synthesis scheme is depicted in Scheme 1. Synthesis of NS_{DAU} (1a) was carried as reported (Levene and Tipson, 1934). Briefly, acetone was conjugated to uridine as ketal in the presence of copper sulfate and conc. sulphuric acid. Synthesis of NL_{DPU} (1b) involved appending the lipid chain of ketone fatty acid, palmitone (16-hentriacontanone), to uridine with the formation of ketal linkage (Taib et al., 2012). The appearance of peaks in ^1H -NMR at δ 1.4-1.2 for the methyl protons and at 114-118 ppm in ^{13}C -NMR for the ketal carbon confirmed the formation of the products. The 5' position was modified as an azide using two-step reaction which involved activation of the hydroxyl using tosyl followed by azidation. The introduction of azide resulted in the up-field shift (from $\delta_{\text{c}} \approx 61$ to $\delta_{\text{c}} \approx 52$ ppm) of the 5' carbon in ^{13}C -NMR. For both ligands, the introduction of the amino group at 5' position was carried by catalytic reduction of the 5'-azide using 10% palladium on activated charcoal. DTPA conjugation with NS_{DAU} and NL_{DPU} was carried as reported. (Chauhan et al., 2014). The yield of formation of $\text{DTPA-NS}_{\text{DAU}}$ (4a) and $\text{DTPA-NL}_{\text{DPU}}$ (4b) was 78% and 64% respectively. The appearance of DTPA characteristic peaks from 30-40 ppm for DTPA-alkyl and 170-180 ppm for DTPA-COOH confirmed the formation. DTPA anhydride tends to conjugate with two moieties resulting in bisamide-DTPA derivatives. In spite of taking an excess of NL_{DPU} , bisamide-DTPA derivative could not be synthesized possibly because of the

steric hindrance. The inability to form bisamide-DTPA derivative, however, acted more favorably. Attachment of two units of nucleolipid would have resulted in very high molecular weight ligand. It is well documented that the chelating ability of the monoamide-DTPA is better than DTPA-bis-derivative. Monoamide-DTPA metal complexes are known to have better pharmacokinetics and in vitro/in vivo stability (Ardestani et al.,2010; Achilefu et al.,2000).



Scheme 1: Reaction conditions (i) DTPA-NS_{DAU}: (R=-CH₃) acetone, copper sulfate, conc. sulphuric acid, stirring 48 h; DTPA-NL_{DPU}: (R=-(CH₂)₁₄-CH₃) 16-hentriacontanone, tosylic acid, triethyl orthoformic acid, THF, reflux, 48 h (ii) tosyl chloride, pyridine-DCM (1:2), ice-cold, o/n (iii) sodium azide, DMF, reflux, 8 h (iv) Pd (10% on activated charcoal), H₂. (v) DTPA-anhydride, triethylamine, DMF, 80°C, 48 h (vi) Na[^{99m}TcO₄], stannous tartrate.

3.2 Physicochemical characterization:

The physicochemical characterization of DTPA-NS_{DAU} and DTPA-NL_{DPU} was based on UV-Vis and potentiometric titrations.

In order to study the effect of lipidization, we compared the UV-Vis spectra of DTPA-NS_{DAU} and DTPA-NL_{DPU}. It is well known that the high and characteristic absorption of modified

nucleic acids and nucleosides in ultraviolet light (at λ_{\max} 260 nm) is due to the absorption of their purine and pyrimidine components (Blackburn et al., 2006). The DTPA-NS_{DAU} and DTPA-NL_{DPU}, both showed an absorption maxima (λ_{\max}) at 260 ± 2 nm (Figure S1)†. The similar molar extinction coefficients of DTPA-NS_{DAU} and DTPA-NL_{DPU} indicated that the long alkyl chain did not impede the extent of interaction of the light with the chromophore. Potentiometric titrations of DTPA-NS_{DAU} and DTPA-NL_{DPU} were carried to study the effect of the lipidic chain. Since we had a ketal linkage, the titration was carried from pH 3-12. DTPA titration is well reported with six inflection points (1.6, 1.8, 2.5, 4.31, 8.5 and 10.5 (Bonin et al., 2016)

Two acid dissociations exist for uridine viz., at 9.4 and 12.52 (Fox et al., 1959). The inflection points of DTPA-NS_{DAU} and DTPA-NL_{DPU} were found to be similar (Table 1).

Table 1: Determination of pKa for DTPA-NS_{DAU} and DTPA-NL_{DPU}

| Ligand | pK1 | pK2 | pK3 | pK4 |
|------------------------|------|-------|-------|--------|
| DTPA-NS _{DAU} | 4.61 | 6.531 | 9.568 | 11.991 |
| DTPA-NL _{DPU} | 5.24 | 6.979 | 9.248 | 10.826 |

3.3 Non-Specific Protein Binding using Florescence spectroscopy:

One of the problems encountered with highly lipophilic compound is protein binding leading to non-specific binding and background signal. In blood, the serum albumin (SA) interacts with the ligand and affects the bioavailability and toxicity of the ligand. Fluorescence quenching based on the decrease of the intrinsic tryptophan fluorescence of albumin due to increase in molecular interactions with the ligand has been used to study the protein binding effects of ligand (Mingxiong et al., 2013).

Fluorescence of the analogues (DTPA-NS_{DAU} and DTPA-NL_{DPU}) was compared with that of bovine serum albumin (BSA). When excited at 280 nm, BSA exhibits fluorescence in the

region 340-350 nm, characteristic for tryptophan of BSA. No fluorescence was observed at 340 nm for the analogues (DTPA-NS_{DAU} and DTPA-NL_{DPU}) when excited at 280 nm (Figure S2)†.

The ligands were incubated with BSA and extent of fluorescence quenching was measured (Figure 4). As $\geq 90\%$ of signal was retained, no appreciable fluorescence quenching was observed for DTPA-NS_{DAU} or DTPA-NL_{DPU} up-to a concentration of 1 mM indicating the suitability of the DTPA-NL_{DPU} for diagnostics at micro-molar concentration. As no shift in emission wavelength was observed for DTPA-NS_{DAU} or DTPA-NL_{DPU}, it can be concluded that the analogues did not have any preferential interaction with tryptophan of BSA and did not affect the conformation of BSA. The pattern of the extent of quenching differed significantly for the analogues at higher concentration. We attribute this effect to two factors (a) steric hindrance and (b) increase in the lipophilic environment. At lower concentration, the quenching extent of DTPA-NL_{DPU} was more governed by steric hindrance than hydrophobic interactions; hence the extent was not very different from that of DTPA-NS_{DAU}. However, with an increase in concentration and associated lipophilicity, the extent of quenching is more for DTPA-NL_{DPU} due to the effect of hydrophobic interactions. Overall, the quenching extent was greater for DTPA-NL_{DPU} as evident by the higher bimolecular quenching constant. The apparent association constants and the number of binding sites (n) are listed in Table 2.

Table 2: Fluorescence quenching parameters for DTPA-NS_{DAU} and DTPA-NL_{DPU}

| | $K_{SV} (\times 10^3 M^{-1})$ | K | N |
|------------------------|-------------------------------|-------|------|
| DTPA-NS _{DAU} | 0.02 | 6.23 | 1.45 |
| DTPA-NL _{DPU} | 0.09 | 10.08 | 0.9 |

3.4 Toxicity assessment:

3.4.1 Haemo-compatibility:

The diagnostic radiotracer is intended to be administered intravenously. Thus, RBCs happen to be first to interact with the ligand. The lysis of RBCs can be an indicator of the blood compatibility of the ligand. Lipophilic drugs or ligands are known to interact with the proteins present in the membranes of erythrocytes (Hinderling et al., 1997) and the extent of interaction in the form of haemolysis can indicate the toxicity of the ligand. It was observed that neither DTPA-NS_{DAU} nor DTPA-NL_{DPU} induce any appreciable haemolysis up to 4 h with 1.7% haemolysis for DTPA-NS_{DAU} and 2% haemolysis for DTPA-NL_{DPU}. These values are comparable with the percent hemolysis of the negative control (1.4%). (Figure 5a)

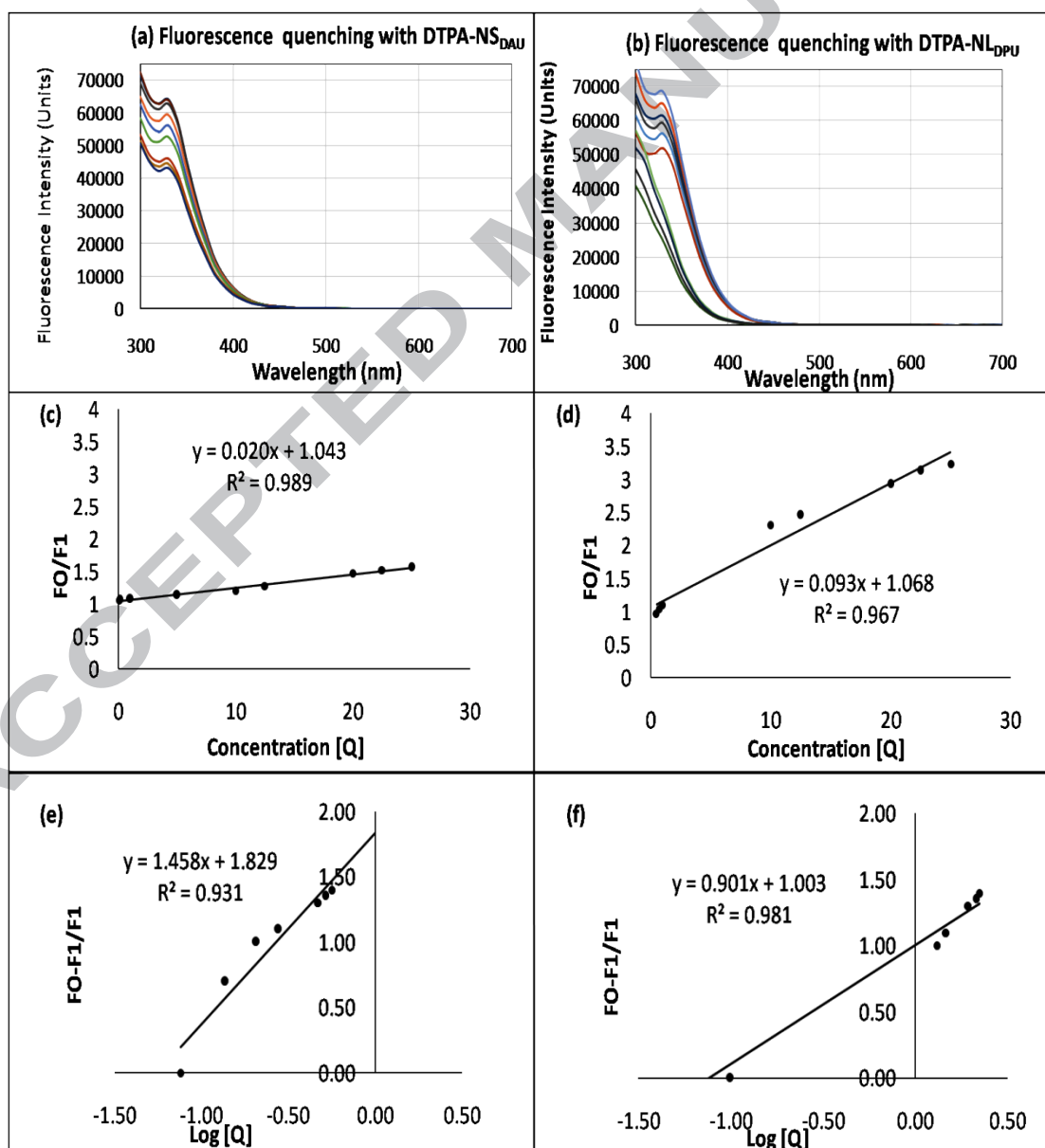


Figure 4: Fluorescence quenching of BSA with ligands : Fluorescence spectra of BSA with experiment with (a) DTPA-NS_{DAU} and (b) DTPA-NL_{DPU} spectra: (c,e and d,f) Stern-Volmer plots for DTPA-NS_{DAU} and DTPA-NL_{DPU} respectively. The λ_{exc} 280 nm and the emission spectra were recorded from 300-700 nm

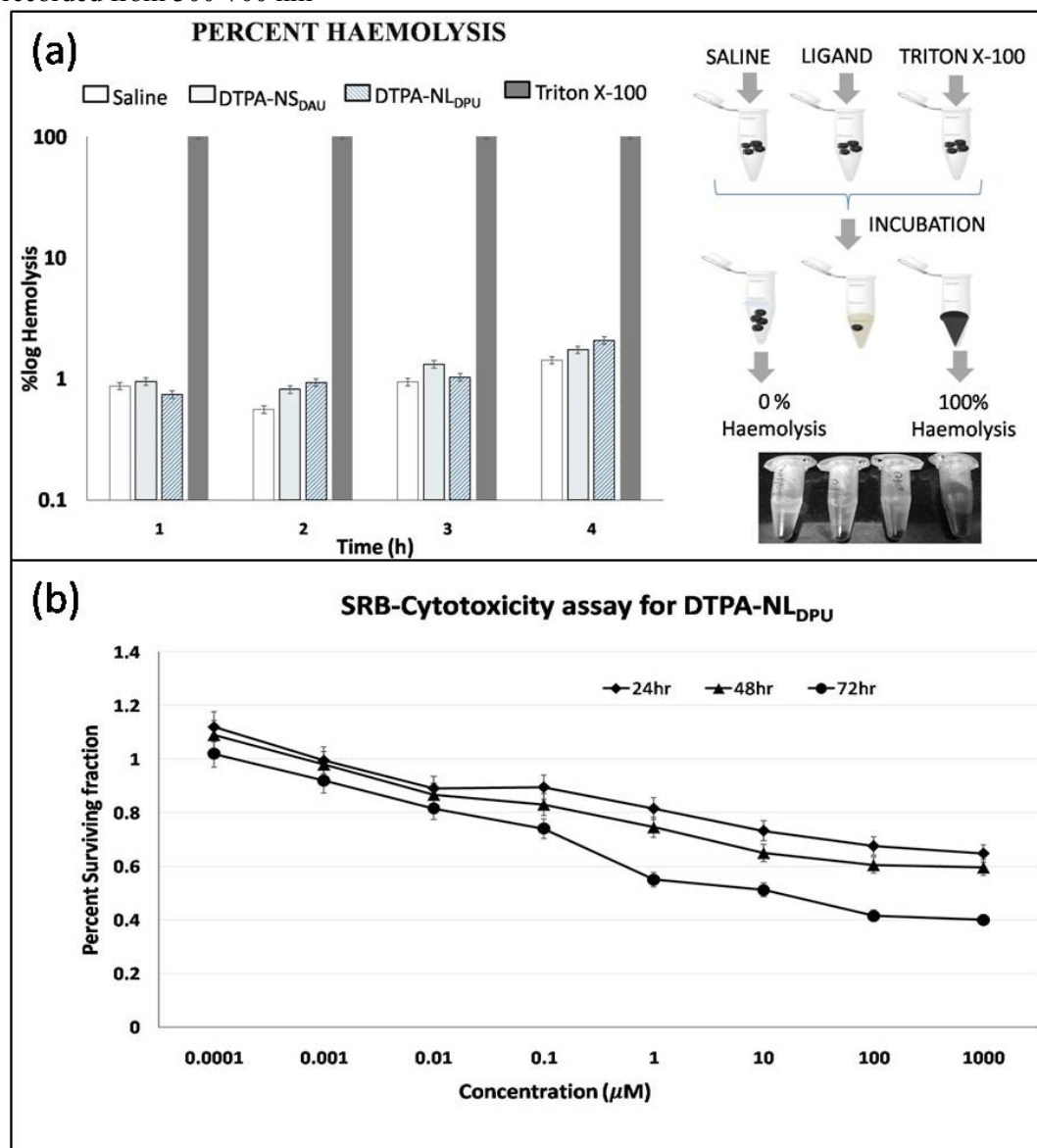


Figure 5: (a) Haemolysis study for DTPA-NS_{DAU} and DTPA-NL_{DPU} in comparison with saline (negative control) and Triton X-100 (positive control). Saline treatment of RBC's shows no haemolysis and Triton X-100 treated RBC's have 100% haemolysis. The data shows no appreciable haemolytic activity of both the compounds DTPA-NS_{DAU} and DTPA-NL_{DPU} up to 4 h. (b) In vitro cytotoxic evaluation of DTPA-NL_{DPU} using SRB assay. Percent surviving fraction plotted against concentration for different treatment time. HEK cells were seeded in 96-well cell plate at a cell density of 5×10^3 . After an intended time of incubation of 24, 48 and 72 h, SRB analysis was performed. The percentage survival was calculated relative to untreated cells and shown as percent survival \pm SD (n = 3).

3.4.2 Cytotoxicity evaluation:

In order to evaluate the cytotoxicity effects of DTPA-NL_{DPU}, Sulforhodamine B (SRB) colorimetric assay was performed (Keepers et al., 1991; Khurana et al., 2015). The cytotoxic effect of DTPA-NL_{DPU} was evaluated on HEK cell line. HEK cell lines have been speculated to have an embryonic neuronal origin, are known to express neuronal proteins and have been used as an alternative for neuronal cells (Madhusudana et al., 2010). Data was plotted for surviving fraction versus concentration of the ligand DTPA-NL_{DPU} for different time points as depicted in Figure 5(b). DTPA-NL_{DPU} was found to be less toxic at concentrations from 0.0001-1000 μM even with an extended treatment of 48 h. A sudden decline in surviving fraction was observed at 10 μM . Nearly 50% cell lysis was observed at 100 μM concentration which gives its IC₅₀ value for 24 and 48 h. The compound showed higher toxicity in 72 h treated HEK-cells with IC₅₀ of 1-10 μM .

3.5 Radio-labelling and stability parameters:

3.5.1 Radio-labelling:

Bifunctional chelating agent DTPA conjugated to ligand (NS_{DAU} and NL_{DPU}) was used for the chelation of ^{99m}Tc. The first step in technetium labeling is the reduction of ^{99m}Tc-pertechnetate, ([^{99m}Tc]-TcO₄⁻), the form in which ^{99m}Tc is eluted from the ^{99m}Technetium generator. Various reducing agents have been reported for the reduction among which stannous salts offer non-toxic and stable preparations (Saha, 2004 ; Spies et al.,2007). Among the stannous salts, chloride has been widely applied. However, when stannous chloride was used for DTPA-NL_{DPU}, the formulation turned opalescent along with low radiolabeling efficiency (85%). Ketal linkages are susceptible to hydrolysis, especially in an acidic environment. Hence, stannous tartrate at pH 8 was used for the reduction and radiolabeling. The ligand labeling was carried at room temperature with optimised labeling parameters (Figure S3)†. DTPA-NS_{DAU} and DTPA-NL_{DPU} were radiolabelled with 95% and 96% radiolabeling efficiency respectively. The radiolabel conjugates were stable for up to 24 h.

^{99m}Tc is known to exhibit various oxidation states, which are dependent on the chelate and pH. In the presence of DTPA, ^{99m}Tc is reported to exist in +3 oxidation states when reduced in acidic solutions (Ebenhan, 2017). However, at neutral/ alkaline pH, ^{99m}Tc exists in +4 oxidation states with DTPA. Since the reduction was carried in neutral pH, the complex formed is neutral and thus suitable for brain penetration.

3.5.2 Lipophilicity:

Empirically, moderate lipophilicity of 1-3 at pH 7.4 along with other criteria ($M_w < 600$ Da and no charge) are used to predict the brain penetration ability of the ligand.²⁸ Lipophilicity calculations of the ligands (DTPA-NS_{DAU} and DTPA-NL_{DPU}) and complexes (^{99m}Tc -DTPA-NS_{DAU} and ^{99m}Tc -DTPA-NL_{DPU}) using octanol-water partition are indicated in Table 3. DTPA-NL_{DPU} has high $M_w \approx 1000$ Da. However, the effect of the high molecular mass of analogues was compensated by the presence of high lipophilicity, thereby facilitating brain entry. This deviation to the empirical rule was also found in brain imaging agents reported earlier (Chaturvedi et al., 2017). The lipophilicity of the ^{99m}Tc labelled complex was found to be 2.3.

Table 3: Log P predictions for DTPA-NS_{DAU} and DTPA-NL_{DPU} before and after radiolabeling with ^{99m}Tc .

| Ligand | Log P | Ligand | Log P |
|------------------------|--------|--|--------|
| DTPA-NS _{DAU} | -0.634 | ^{99m}Tc - DTPA-NS _{DAU} | -0.235 |
| DTPA-NL _{DPU} | 1.734 | ^{99m}Tc -DTPA-NL _{DPU} | 2.356 |

When the ligand is lipophilic, non-specific protein binding can play an important role in its bio-distribution. Strong binding to serum protein can delay blood clearance, resulting in a low signal to background ratio. The stability of complexes ^{99m}Tc -DTPA-NS_{DAU} and ^{99m}Tc -DTPA-NL_{DPU} was compared by incubating the complexes with freshly extracted human serum. The

samples were analysed using ITLC and stability was the extent of associated radioactivity. On incubation with human serum, a slow degradation was observed with approximately 92% ^{99m}Tc -DTPA-NS_{DAU} and 89% ^{99m}Tc -DTPA-NL_{DPU} intact tracer present even after 24 h (Figure S 27†).

3.5.3 Trans-chelation using Cysteine challenge studies

It is known that high concentration of thiol-containing cysteine ($\approx 10\mu\text{M}$) is present in serum which can bind to ^{99m}Tc (Hnatowich et al., 1993). The complexes (^{99m}Tc -DTPA-NS_{DAU} and ^{99m}Tc -DTPA-NL_{DPU}) were incubated at 1: 25, 1:50 and 1: 100 molar ratios with cysteine for 2 h at 37 °C. The results confirmed that ^{99m}Tc -DTPA-NS_{DAU} and ^{99m}Tc -DTPA-NL_{DPU} were stable and approximately 95% of the radioactivity remained bound to DTPA-NS_{DAU} and DTPA-NL_{DPU} even at 100 mM concentration of cysteine. Further, it was noted that both the complexes had comparable stability towards trans-chelation with 4.3% of ^{99m}Tc -DTPA-NS_{DAU} and 3.3 % of ^{99m}Tc -DTPA-NL_{DPU} dissociated after 2 h incubation with 100 times more cysteine concentration than the complex. (Figure 6a)

3.6 In Vivo Evaluation and Pharmacokinetics

3.6.1 Blood Clearance

In order to understand the distribution and elimination parameters of the complexes (^{99m}Tc -DTPA-NS_{DAU} and ^{99m}Tc -DTPA-NL_{DPU}), the time variation of radiotracer concentration in blood was monitored. Both complexes (^{99m}Tc -DTPA-NS_{DAU} and ^{99m}Tc -DTPA-NL_{DPU}) conform to the first order kinetics with two distinct phases (biphasic profile corresponding to distribution and elimination), a feature in the two-compartment model (Figure 9: Dhillon et al., 2006). Pharmacokinetic parameters were evaluated as shown in Table 4. The analogues cleared rapidly from the blood with 50 % total blood activity remaining at time 15 min (^{99m}Tc -DTPA-NS_{DAU}) and 120 min (^{99m}Tc -DTPA-NL_{DPU}).

Table 4: Pharmacokinetic parameters for ^{99m}Tc -DTPA-NS_{DAU} and ^{99m}Tc -DTPA-NL_{DPU}

| Parameters | $^{99m}\text{Tc-DTPA-NS}_{\text{DAU}}$ | $^{99m}\text{Tc-DTPA-NL}_{\text{DPU}}$ |
|---|--|--|
| Dose (mg/kg) | 0.08 mg/kg | 0.08 mg/kg |
| % Radioactivity at time zero | 50.93% | 38.23 % |
| α : distribution rate constant | 0.0463 | 0.0149 |
| β : elimination rate constant | 0.0006 | 0.0005 |
| $t_{1/2}(\alpha)$: initial disposition half-life | 14.96 min | 46.5 min |
| $t_{1/2}(\beta)$: terminal elimination half-life | 1155 min | 1386 min |
| Vd: volume of distribution | 377 mL | 423 mL |

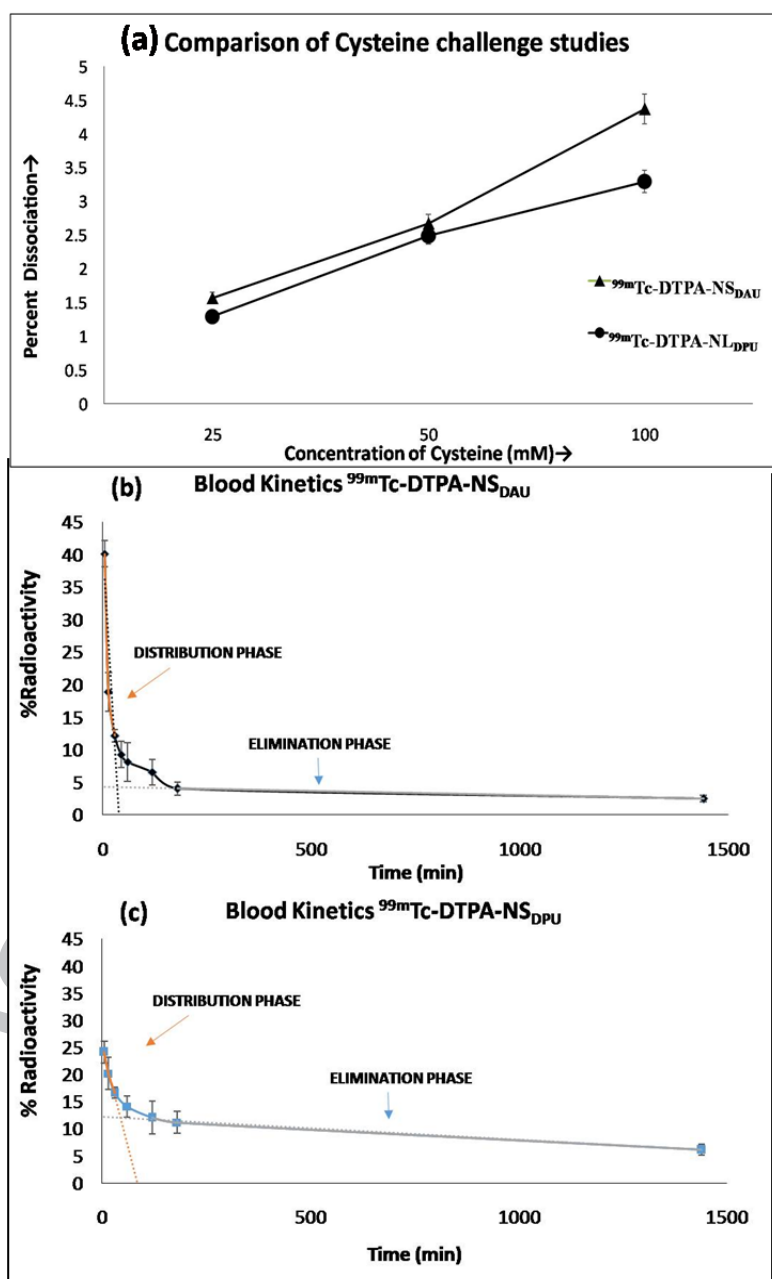


Figure 6: (a) Cysteine challenge studies of $^{99m}\text{Tc-DTPA-NS}_{\text{DAU}}$ and $^{99m}\text{Tc-DTPA-NL}_{\text{DPU}}$ when incubated with varying concentrations of cysteine for 2 h at 37°C. The results indicate no appreciable trans-chelation of complex bound ^{99m}Tc with cysteine (b) Blood kinetics profile for $^{99m}\text{Tc-DTPA-NS}_{\text{DAU}}$ and (c) Blood kinetics profile for $^{99m}\text{Tc-DTPA-NL}_{\text{DPU}}$

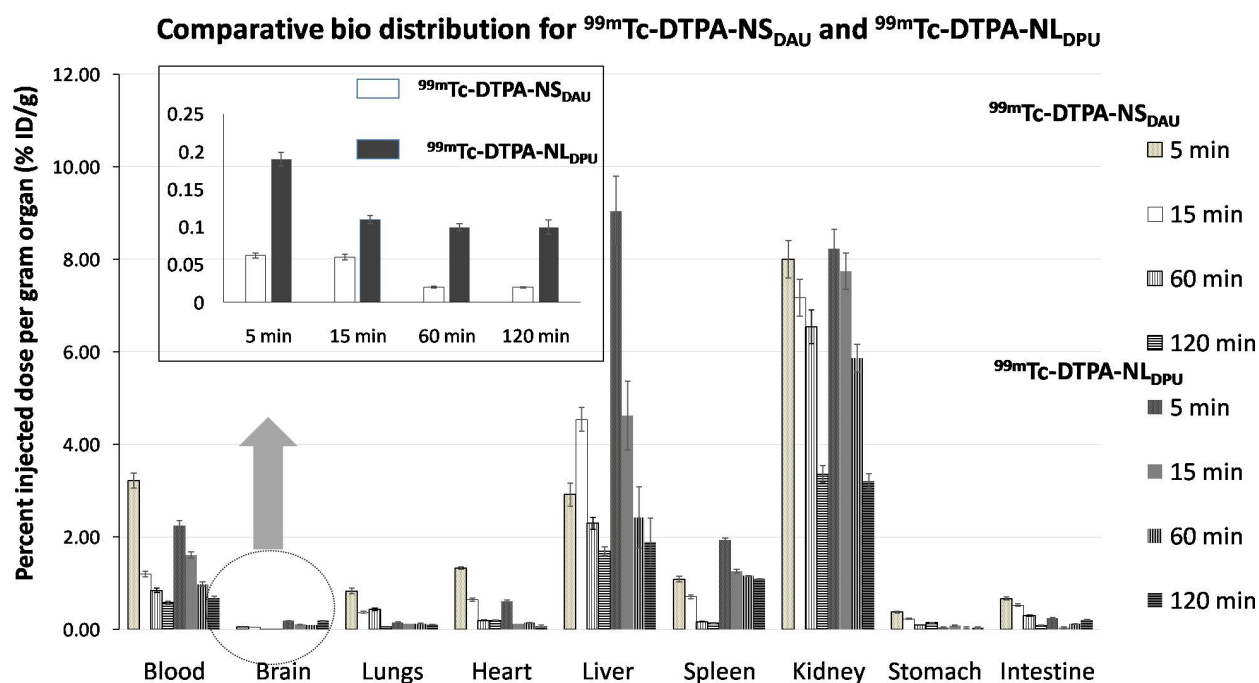


Figure 7: Comparative bio distribution of $^{99m}\text{Tc-DTPA-NS}_{\text{DAU}}$ and $^{99m}\text{Tc-DTPA-NL}_{\text{DPU}}$, performed in BALB/c mice: data from 4 groups of 3 mice each expressed as a mean % ID ($n = 3$). Organs analysed for radioactive counts after required time points post i.v. injection via the tail vein.

In comparison to $^{99m}\text{Tc-DTPA-NS}_{\text{DAU}}$, $^{99m}\text{Tc-DTPA-NL}_{\text{DPU}}$ exhibited greater circulation time. This increase in circulation time can be attributed to the presence of lipid chain. Higher the lipophilicity, higher is the chance of the interaction with protein and uptake/accumulation by RBCs. However, as shown above, the protein binding of nucleolipidic analogue though more than nucleoside, was not significant for concentrations used in diagnostics. Similarly, the toxic effects on RBC's were not found to be substantial.

3.6.2 Bio-distribution Studies

3.6.2.1 Bio-distribution in Normal Mice:

Bio-distribution studies in normal mice were carried to compare the uptake of ligands in the brain and also study the variation in the pattern of distribution as a result of

lipidization. The complexes ($^{99m}\text{Tc-DTPA-NS}_{\text{DAU}}$ and $^{99m}\text{Tc-DTPA-NL}_{\text{DPU}}$) were administered in mice intravenously, and their uptake was assessed in different organs at different time points after sacrificing the animal. The bio-distribution graphs are given in Figure 7. At 5 min post injection, brain uptake of 0.19 ± 0.01 % I.D/g was obtained for $^{99m}\text{Tc-DTPA-NL}_{\text{DPU}}$ compared to 0.06 % I.D/g for $^{99m}\text{Tc-DTPA-NS}_{\text{DAU}}$ (uptake ratio 3.1). The accumulation in liver and kidney is in accordance with reported routes of excretion viz., hepatobiliary (liver, spleen) and renal (kidney) routes for DTPA complexes. Liver and spleen uptake of $^{99m}\text{Tc-DTPA-NL}_{\text{DPU}}$ was higher than $^{99m}\text{Tc-DTPA-NS}_{\text{DAU}}$ due to the lipophilic character. The absence of activity in stomach confirms the in vivo stability of the ligands. Activity in the stomach is associated with free technetium available in the body as a result of de-complexation. The bio-distribution data (Figure 7) also indicates washout of most of the radioactivity ($< 2\%$ ID/g) from the tissues and organs within 2 h except kidney which is associated with renal route of excretion for DTPA derivatives.

3.6.2.2 Scintigraphy Imaging in intracranial Xenograft mice:

Further, to ascertain the brain tumor uptake, intracranial xenograft of brain malignant glioma cells (U87-MG) was developed as reported previously (Ozawa and James, 2010). After appropriate model evaluation based on histology of brain slices (Figure S27)†, the mice were administered with the complexes ($^{99m}\text{Tc-DTPA-NS}_{\text{DAU}}$ and $^{99m}\text{Tc-DTPA-NL}_{\text{DPU}}$). Imaging studies were carried in the intracranial U87-MG xenograft using $^{99m}\text{Tc-DTPA-NS}_{\text{DAU}}$ and $^{99m}\text{Tc-DTPA-NL}_{\text{DPU}}$ which clearly showed an appreciable uptake of $^{99m}\text{Tc-DTPA-NL}_{\text{DPU}}$ at the tumor site in brain (Figure 8). No significant uptake was observed for $^{99m}\text{Tc-DTPA-NS}_{\text{DAU}}$ (as shown in Figure S29)†. The non-accumulation of $^{99m}\text{Tc-DTPA-NS}_{\text{DAU}}$ could be attributed to the negative Log P value (-0.235) which indicates hydrophilic nature of the non-lipidic compound.

Semiquantitative analyses indicated 4.452 ± 1.2 counts/mm² in intracranial tumor bearing mouse brain (n=5) and abdomen uptake was found to be 24.099 ± 3.8 counts/mm².

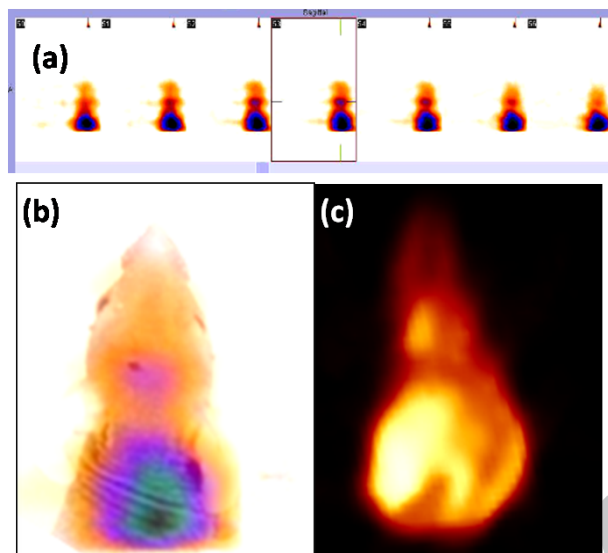


Figure 8: Scintigraphy image of intracranial xenograft mice (a) panel showing static tomographic acquisitions at 1h p.i. (b) superimposed image of athymic mice with scintigraphic scan showing ^{99m}Tc-DTPA-NL_{DPU} accumulation at intracranial U87-MG xenograft on left side of the brain (c) 3D image of the uptake at the tumor site in the left hemisphere of the brain of athymic mice.

4. CONCLUSIONS

Early detection in brain anomalies, namely tumor is restricted due to the inability of the present class of tracers to permeate an intact blood-brain barrier. The work was designed with the aim to develop a delivery system that can cross the BBB. Brain permeation is a complex interplay of various parameters with lipophilicity and molecular weight being the main variables. In search for molecules that can have the potential to cross the intact BBB, we took leads from the success of nucleolipids as cell penetrating agents attributed to their lipophilicity. In this contribution, we have demonstrated that the nucleolipids are better able to cross an intact BBB and accumulate in the brain. Even though lipophilic with high molecular weight, nucleolipids were found to be non-toxic and can certainly be used in

diagnostics. The exact mechanism of BBB permeation needs to be investigated. Further work of the effect of length and nature of the lipid chains, linkages, and chelators on brain permeation ability of the nucleosides will aid in the fine tuning of design considerations. This work, possibly the first of the kind emphasizes on the suitability of the nucleolipids as brain permeation agents with application in diagnostic imaging.

ASSOCIATED CONTENT

Supporting Information

Synthesis and characterization of non-lipidic nucleoside (DTPA-NS_{DAU}) and nucleolipid (DTPA-NL_{DPU}), UV-Vis calibration curves of DTPA-NS_{DAU} and DTPA-NL_{DPU}, Fluorescence spectra of DTPA-NS_{DAU} and DTPA-NL_{DPU} and detailed radiolabeling procedure of DTPA-NS_{DAU} and DTPA-NL_{DPU} with ^{99m}Tc, serum stability, Histological analysis

CONFLICT OF INTEREST

The authors declare no conflict of interest.

ACKNOWLEDGMENTS

This research was supported in part by DRDO, Ministry of Defence, under research and development project INM-311 and DST funded project SR/NM/NS-1046/2015(G). We greatly appreciate and thank Dr. A.K Singh, Director INMAS, Delhi for his continuous support and for providing the necessary facilities. The authors also thank Prof. Dr. P Sen, School of Physical Sciences, JNU, Delhi for his expertise that greatly assisted the research.

REFERENCES

1. Achilefu, S.; Wilhelm, R.R.; Jimenez, H.N.; Schmidt, M.A.; Srinivasan, A. A new method for the synthesis of tri-tert-butyl diethylenetriaminepentaacetic acid and its derivatives. *J Org Chem.* **2000**, 65(5), 1562-5. doi: 10.1021/jo991453t
2. Alauddin, M.M. Nucleoside-based probes for imaging tumor proliferation using positron emission tomography. *J. Labelled Comp. Radiopharm.* **2013**, 56(3-4), 237-43. doi: 10.1002/jlcr.3003.
3. Allain, V., Bourgaux, C., Couvreur, P. Self-assembled nucleolipids: from supramolecular structure to soft nucleic acid and drug delivery devices. *Nucleic Acids Res*, 2012, 40(5), 1891–1903. doi:10.1093/nar/gkr681
4. Ardestani, M.S.; Arabzadeh, A.J.; Heidari, Z.; Hosseinzadeh, A.; Ebrahimi, H.; Hashemi, E.; Mosayebnia, M.; Shafiee-Alavidjeh, M.; Alavi, A.; Babaei, M.H.; Rahmim, A. Novel and facile methods for the synthesis of DTPA-mono-amide: a new completely revised strategy in radiopharmaceutical chemistry. *J. Radioanal. Nucl. Chem.* **2010**, 283(2), 447-55. doi: 10.1007/s10967-009-0414-y
5. Baillet, J.; Desvergnès, V.; Hamoud, A.; Latxague, L.; Barthélémy, P. Lipid and Nucleic Acid Chemistries: Combining the Best of Both Worlds to Construct Advanced Biomaterials. *Adv. Mater.* **2018**, 30(11), doi: 10.1002/adma.201705078

6. Basu, S; Alavi A. Molecular imaging (PET) of brain tumors. *Neuroimaging Clin. N. America.* **2009**, *19(4)*, 625-46. doi: 10.1016/j.nic.2009.08.012.
7. Bedikian, A.Y.; DeConti, R.C.; Conry ,R.; Agarwala, S.; Papadopoulos,N.; Kim,K.B. Ernstoff M. Phase 3 study of docosahexaenoic acid–paclitaxel versus dacarbazine in patients with metastatic malignant melanoma. *Ann. Oncol.*, **2010**, *22(4)*, 787-93. doi: 10.1093/annonc/mdq438.
8. Blackburn, G. M. DNA and RNA structure In *Nucleic Acids in Chemistry and Biology*, 3 rd ed; Blackburn, G.M.; Gait, M. J.; Loakes, D.; Williams D. M. (Eds.). Royal Society of Chemistry, **2006**; Chapter 2, pp 13-76.
9. Bonin, L.; Aupiais, J.; Kerbaa, M.; Moisy, P.; Topin, S.; Siberchicot, B. Revisiting actinide–DTPA complexes in aqueous solution by CE-ICPMS and ab initio molecular dynamics. *RSC Adv.* **2016**, *6(67)*,62729-41. doi:10.1039/C6RA08121E
10. Chaturvedi, S.; Kaul, A.; Hazari ,P.P.; Mishra, A.K.; Mapping neuroreceptors with metal-labeled radiopharmaceuticals. *MedChemComm.* **2017**, *8(5)*, 855-70. doi:10.1039/C6MD00610H
11. Chaturvedi, S.; Mishra, A.K. Small molecule radiopharmaceuticals—a review of current approaches. *Front. Med*, **2016**, *3*, 5. doi.org/10.3389/fmed.2016.00005
12. Chauhan, K.; Datta, A.; Adhikari, A.;Chuttani, K.; Singh, A.K; Mishra ,A.K. 68 Ga based probe for Alzheimer's disease: synthesis and preclinical evaluation of homodimeric chalcone in β -amyloid imaging. *Org. Biomol. Chem.*, 2014,*12*, 7328-7337. doi:10.1039/C4OB00941J
13. Chen, W.; Cloughesy, T.; Kamdar, N.; Satyamurthy, N.; Bergsneider, M.; Liau, L.; Mischel, P.; Czernin, J.; Phelps, M.E.; Silverman, D.H. Imaging proliferation in brain tumors with 18F-FLT PET: comparison with 18F-FDG. *J. Nucl. Med.* **2005**, *46(6)*, 945-52.

14. Demetrius, L. A.; Magistretti, P. J.; Pellerin, L. Alzheimer's disease: the amyloid hypothesis and the Inverse Warburg effect. *Front. Physiol.* **2014**, *5*, 522-610. doi:10.3389/fphys.2014.00522
15. Dhillon, S.; Kostrzewski, A. (Eds). Clinical pharmacokinetics. Pharmaceutical Press; 2006.
16. Di Galleonardo, V.; Wilson, D.M.; Keshari, K.R. The potential of metabolic imaging. *Semin. Nucl. Med.* **2016**, *46(1)*, 28-39. doi: 10.1053/j.semnuclmed.2015.09.004.
17. Dumoga, S.; Rai, Y.; Bhatt, A.N.; Tiwari, A.K.; Singh, S.; Mishra, A.K.; Kakkar, D. Block Copolymer Based Nanoparticles for Theranostic Intervention of Cervical Cancer: Synthesis, Pharmacokinetics, and in Vitro/in Vivo Evaluation in HeLa Xenograft Models. *ACS Appl Mater Interfaces.* **2017**, *9(27)*, 22195-211. doi: 10.1021/acsami.7b04982.
18. Ebenhan, T.; Wagener C. Radiochemistry In *Imaging Infections: From Bench to Bedside*, Springer International Publishing, Jain, S.K. (Ed.), 2017; Chapter 4, pp 77-131.
19. Fox, J.J.; Wempfen, I. Pyrimidine Nucleosides In *Advances in Carbohydrate Chemistry*, Volume 14, Wolfrom, M.L. (Ed.) Academic Press: New York, **1959**; Chapter 5, pp 300
20. Gissot, A.; Camplo, M.; Grinstaff, M. W.; Barthelemy, P.; Nucleoside, nucleotide and oligonucleotide based amphiphiles: a successful marriage of nucleic acids with lipids. *Org. Biomol. Chem.*, **2008**, *6(8)*, 1324-33. doi: 10.1039/b719280k
21. Gissot, A.; Di Primo, C.; Bestel, I.; Giannone, G.; Chapuis, H.; Barthelemy, P. Sensitive liposomes encoded with oligonucleotide amphiphiles: a biocompatible switch. *Chem. Commun.*, **2008**, (43), 5550-2. doi:10.1039/B812398E

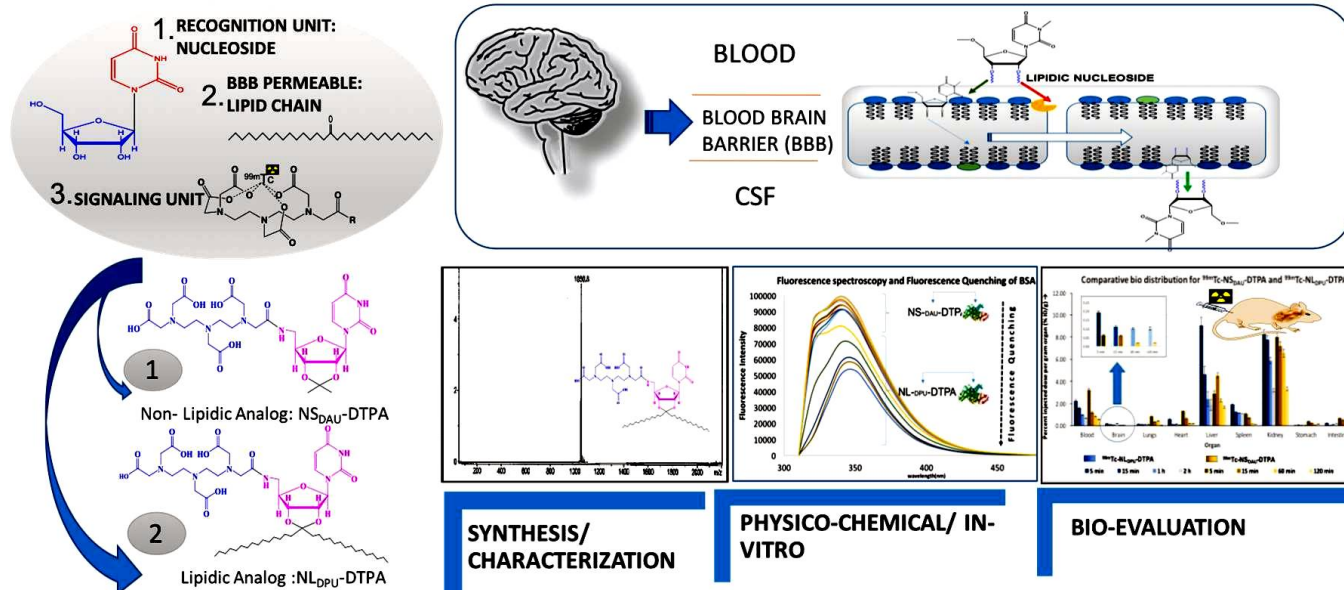
22. Gleeson, L.E.; Sheedy, F.J. Metabolic reprogramming & inflammation: fuelling the host response to pathogens. *Semin. Immunol.* **2016**, *28* (5), 450-468. doi: 10.1016/j.smim.2016.10.007.
23. Herbert, B.S.; Gellert, G.C.; Hochreiter, A.; Pongracz, K.; Wright, W.E.; Zielinska, D.; Chin, A.C.; Harley, C.B.; Shay, J.W.; Gryaznov, S.M.; Lipid modification of GRN163, an N3'→P5' thio-phosphoramidate oligonucleotide, enhances the potency of telomerase inhibition. *Oncogene.* **2005**, *24*(33), 5262-68. doi:10.1038/sj.onc.1208760
24. Hinderling, P.H. Red blood cells: a neglected compartment in pharmacokinetics and pharmacodynamics. *Pharmacol. Rev.* **1997**, *49*(3), 279-95.
25. Hnatowich, D.J.; Mardirossian, G.; Rusckowski, M.; Fogarasi, M.; Virzi, F.; Winnard, P. Directly and Indirectly Technetium-99m-Labeled Antibodies A—Comparison of In Vitro and Animal In Vivo Properties. *J. Nucl. Med.* **1993**, *34*(1), 109-19.
26. Kao, C. H.; Waki, A.; Sassaman, M.B.; Jagoda, E. M.; Szajek, L. P.; Ravasi, L.; Shimoji, K.; Eckelman, W. C. Evaluation of [76Br]FBAU 3',5'-dibenzoate as a lipophilic prodrug for brain imaging. *Nucl. Med. Biol.*, **2002**, *29*(5), 527-35. doi: 10.1016/S0969-8051(02)00324-4
27. Keepers, Y.P.; Pizao, P.E.; Peters, G.J.; van Ark-Otte, J.; Winograd, B.; Pinedo, H.M. Comparison of the sulforhodamine B protein and tetrazolium (MTT) assays for in vitro chemosensitivity testing. *Eur. J. Cancer.* **1991**, *27*(7), 897-900. doi: 10.1016/0277-5379(91)90142-Z
28. Khurana, H.; Meena, V.K.; Prakash, S.; Chuttani, K.; Chadha, N.; Jaswal A.; Dhawan, D.K.; Mishra, A.K., Hazari, P.P. Preclinical Evaluation of a Potential GSH Ester Based PET/SPECT Imaging Probe DT(GSHMe)₂ to Detect Gamma Glutamyl

- Transferase Over Expressing Tumors. *PLoS One*, **2015**, *10*(7): e0134281. doi: 10.1371/journal.pone.0134281
29. Langen, K-Josef ; Galldiks, N. PET imaging of Brain Tumors In *Brain Tumor Imaging*, Hattingen, E.; Pilatus, U.(Eds.), Springer, Berlin, Heidelberg, 2016; Chapter 7, 121-134. doi.org/10.1007/174_2013_937
30. Lansakara-P, D. S.;Rodriguez, B. L.;Cui, Z. Synthesis and in vitro evaluation of novel lipophilic monophosphorylated gemcitabine derivatives and their nanoparticles. *Int. J. Pharm.* , **2012**, *429*(1-2), 123–134. doi:10.1016/j.ijpharm.2012.03.014
31. Levene, P.A.; Tipson ,R.S. The partial synthesis of ribose nucleotides I. Uridine 5-phosphoric acid. *Journal of Biological Chemistry*. **1934**, *106*(1):113-24.
32. Levy, P.; Bartosch, B. Metabolic reprogramming: a hallmark of viral oncogenesis. *Oncogene*. **2016**, *35*(32), 4155-4164. doi: 10.1038/onc.2015.479.
33. Li, H.F.;Winkeler, A.; Moharram, S.; Knaus, E.E.;Dittmar, K.; Stockle, M.;Heiss, W.D.; Wiebe, L.I.;Jacob, A.J. In vivo evaluation of the uptake of [123I] FIAU,[123I] IVFRU and [123I] IVFAU by normal mouse brain: potential for noninvasive assessment of HSV-1 thymidine kinase gene expression in gliomas. *Nucleosides Nucleotides Nucleic Acids*, **2008**, *27*(1), 57-66. doi:10.1080/15257770701571933.
34. Li, M.;Selvin, P.R. Luminescent polyaminocarboxylate chelates of terbium and europium: the effect of chelate structure. *J. Am. Chem. Soc.*, **1995**, *117*(31), 8132-8. doi: 10.1021/ja00136a010.
35. Liu, S. Bifunctional Coupling Agents for Radiolabeling of Biomolecules and Target-Specific Delivery of Metallic Radionuclides. *Adv. Drug Deliv/ Rev.*, **2008**, *60*(12), 1347–1370. doi:10.1016/j.addr.2008.04.006
36. Madhusudana, S.N.; Sundaramoorthy, S.; Ullas, P.T. Utility of human embryonic kidney cell line HEK-293 for rapid isolation of fixed and street rabies viruses:

- comparison with Neuro-2a and BHK-21 cell lines. *Int. J. Infect. Dis.* **2010**, *14*(12), e1067-71. doi: 10.1016/j.ijid.2010.07.004
37. Meyer, J.P.; Probst, K.C.; Westwell, A.D. Radiochemical synthesis of 2'-[18F]-labelled and 3'-[18F]-labelled nucleosides for positron emission tomography imaging. *J. Labelled Comp. Radiopharm.* **2014**, *57*(5), 333-37. doi:10.1002/jlcr.3197
38. Mingxiong, T.; Weijiang, L.; Xujian, L.; Yunqiong, G. Fluorescence Spectroscopy Study on the Interaction between Evodiamine and Bovine Serum Albumin, *Journal of Chemistry*, **2013**, vol. 2013, Article ID 308054, doi:10.1155/2013/308054
39. Miyagawa, T.; Gogiberidze, G.; Serganova, I.; Cai, S.; Balatoni, J.A.; Thaler, H.T.; Ageyeva, L.; Pillarsetty, N.; Finn, R.D.; Blasberg, R.G. Imaging of HSV-tk Reporter gene expression: comparison between [18F] FEAU, [18F] FFEAU, and other imaging probes. *J Nucl Med.* **2008**, *49*(4), 637-48. doi: 10.2967/jnumed.107.046227.
40. Mizuno, A.; Cherepanov, S. M.; Kikuchi, Y.; Fakhrul, A.A.; Akther, S.; Deguchi, K.; Yoshihara, T.; Ishihara, K.; Shuto, S.; Higashida, H. Lipo-oxytocin-1, a Novel Oxytocin Analog Conjugated with Two Palmitoyl Groups, Has Long-Lasting Effects on Anxiety-Related Behavior and Social Avoidance in CD157 Knockout Mice. *Brain Sci.*, **2015**, *5*(1), 3-13. doi:10.3390/brainsci5010003
41. Ozawa, T., James, C.D. Establishing Intracranial Brain Tumor Xenografts With Subsequent Analysis of Tumor Growth and Response to Therapy using Bioluminescence Imaging, *Journal of visualized experiments: JoVE*. 2010(41).
42. Pysz, M.A.; Willmann, J.K. Applications of Molecular Small Animal Imaging in Oncology In *Molecular Imaging of Small Animals: Instrumentation and Applications*, Zaidi H.(Ed.), Springer, 2014; Chapter 21, 602-605
43. Robinson, P.J.; Noronha, J.; DeGeorge, J.J.; Freed, L.M.; Nariai, T.; Rapoport, S.I. A quantitative method for measuring regional in vivo fatty-acid incorporation into and

- turnover within brain phospholipids: review and critical analysis. *Brain Res Brain Res Rev.* **1992**, *17*(3), 187-214. doi.:10.1016/0165-0173(92)90016-F
44. Rosemeyer, H. Nucleolipids: natural occurrence, synthesis, molecular recognition, and supramolecular assemblies as potential precursors of life and bioorganic materials. *Chem Biodivers.* **2005**, *2*(8), 977-1063. doi: 10.1002/cbdv.200590082
45. Saha, G.B. In *Fundamentals of Nuclear Pharmacy.*, 1st ed.; Springer-Verlag: New York, 2004.
46. Scheidt, H.A.;Flasche ,W.; Cismas, C.; Rost, M.; Herrmann, A.; Liebscher ,J.; Huster ,D. Design and application of lipophilic nucleosides as building blocks to obtain highly functional biological surfaces. *J. Phys. Chem. B*, **2004**,*108*(41), 16279-87. doi: 10.1021/jp046606h
47. Schwarzenberg, J; Radu, C.G.; Benz, M;Fueger, B;Tran, A.Q.; Phelps, M.E.;Witte, O.N.;Satyamurthy, N; Czernin, J; Schiepers ,C. Human biodistribution and radiation dosimetry of novel PET probes targeting the deoxyribonucleoside salvage pathway. *Eur. J. Nucl. Med. Mol. Imaging.* **2011**, *38*(4), 711-21. doi: 10.1007/s00259-010-1666-z.
48. Spector, A.A.; Yorek, M.A. Membrane lipid composition and cellular function. *J Lipid Res.* **1985**, *26*(9), 1015-35.
49. Spies, H.; Pietzsch, H.J. Stannous chloride in the preparation of ^{99m}Tc pharmaceuticals. In *Technetium-99m Pharmaceuticals*, Springer Berlin Heidelberg, 2007; pp 59-66.
50. Taïb, N.; Aimé, A.; Moreau, L.;Camplo ,M.; Houmadi, S.; Desbat, B.; Laguerre, M.; Grinstaff, M.; Bestel, I.; Barthélémy ,P. Formation of Supramolecular Systems via Directed Nucleoside-lipid Recognition, *J. Colloid Interface Science*, **2012**, *377*(1), 122-30 doi: 10.1016/j.jcis.2012.03.041

51. Tehrani, O.S.; Shields A.F. PET imaging of proliferation with pyrimidines. *J Nucl Med.* **2013**, *54(6)*, 903-12. doi: 10.2967/jnumed.112.112201
52. Zaro, J. L. Lipid-Based Drug Carriers for Prodrugs to Enhance Drug Delivery. *The AAPS Journal*, **2015**, *17(1)*, 83–92. <http://doi.org/10.1208/s12248-014-9670-z>:
53. Zhu, S., Wonganan, P., Lansakara-P, D. S. P., O'Mary, H. L., Li, Y., Cui, Z. The effect of the acid-sensitivity of 4-(N)-stearoyl gemcitabine-loaded micelles on drug resistance caused by RRM1 overexpression. *Biomaterials*, **2013**, *34(9)*, 2327–2339. doi:10.1016/j.biomaterials.2012.11.053
54. Zolle, P. O.; Bremer, Gy. Jánoki, Monographs of ^{99m}Tc Pharmaceuticals In *Technetium-99m Pharmaceuticals: Preparation and Quality Control in Nuclear Medicine*, Zolle, I. (Ed.), Springer-Verlag Berlin Heidelberg, 2007, pg 299-300



EVALUATION OF BBB PERMEABLE NUCLEOLIPID (NL_{DPU}): A DI-C15-KETALISED PALMITONE APPENDED URIDINE AS NEURO- TRACER FOR SPECT

1. Nucleolipid- potential ligand to cross the intact BBB and application in early diagnosis.
2. Synthesis of non-lipidic and di-C15 ketalised lipidic uridine
3. Comparative physico-chemical, biocompatibility and pharmacological evaluation
4. Brain uptake of lipidic uridine three times higher than non-lipid uridine.
5. First-of-its-kind work presents biocompatible nucleolipid as ^{99m}Tc -SPECT neuro-tracer

CONFLICT OF INTEREST

The authors declare no conflict of interest.

